J. Indian Inst. Sci. 63 (A), Sept. 1981, Pp. 183–211

Erosion studies due to liquid jet impingement with plain and cavitating jets

K. S. JANAKIRAM* AND B. C. SYAMALA RAO
Department of Civil Engineering, Indian Institute of Science, Bangalore 560 012, India.

Received on September 11, 1981.

Abstract

Experimental investigations were made on the characteristics of erosion resulting from the impingement of liquid jets ; six plain jets and four jets with cavitation inducers in a velocity range of 5 to 45 m/s. A detailed dimensional analysis of the several parameters governing liquid impingement erosion is presented. The growth of the jet size with stand-off distance for plain jets and the erosion characteristics due to variation in stand-off distance are also discussed. The normalized erosion rate increased with jet velocity and approached a constant value at higher jet velocities. The erosion rate decreased rapidly and then remained approximately constant with an increase in cavitation number. The erosion rate increased faster with frequency of impingement than with increase in jet velocity. A maximum value in peak erosion rate occurred around angles of impingement of 25 to 40 deg. The erosion rate-time curves for impingement of jets with cavitation inducers did not show the incubation and accumulation zones significantly. The cavity patterns obtained in the case of jets with cavitation inducers are similar to those reported in cavitation studies. The length and width of cavity increase with decrease in cavitation number.

Key words : Impingement, cavitation, erosion, erosion resistance characteristics.

Introduction

In recent years, there has been considerable interest in the utilization of liquid jets for drilling, cutting, tunnelling, mining and for mixing process applications. Jet cutting processes in industry are of importance only in special cases, like cutting of very hard or very soft materials. The process of damage or breakage by water jetting is a complex phenomenon involving the propagation of stress waves, compression, cratering large scale cracking, shear fracture and erosion[1–4].

Present address : Technology Utilisation Division, Department of Science and Technology, New Delhi 110 016, India.

Liquid impingement effects are observed in case of steam turbine blades operating under 'wet' steam conditions. As steam expands, a decrease in pressure takes place and the condensed steam forms droplets which impinge on the blades and cause erosion. Heavy damage on Pelton wheel buckets due to the impingement of high speed water jets was reported in many instances[5,6]. Though the buckets are designed to avoid cavitation, roughening of the surface due to the erosion caused by impact may lead to serious problem resulting in drop in efficiency and increased wear. The utilization of improved metals and coatings has not helped much in overcoming erosion hazards[7,8]. Erosion has been a serious problem in equipment other than rotating machinery, such as in wet steam extraction pipes and in the cross-over pipes where entrained droplets do not follow the streamlines and impinge on the material surface[9,10].

2. Experimental equipment

The experimental test rig (fig. 1) consists of two liquid jets which issue from a pair of identical nozzles (fig. 2) impinging on to four test specimens mounted at equal spacings on the periphery of a rotating disc (figs. 3a, b.). The test specimens of size

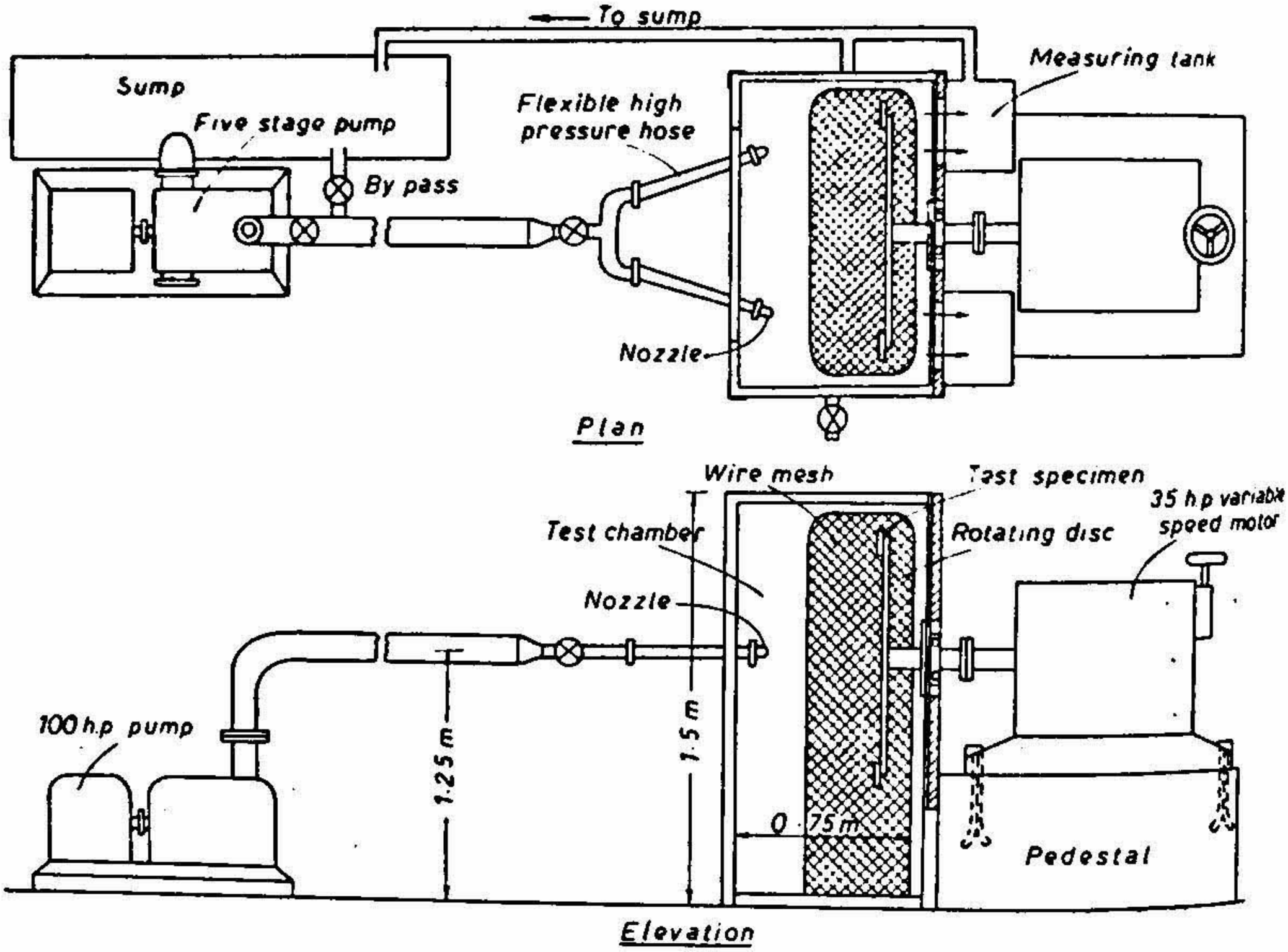

FIG. 1. Liquid impingement test rig.

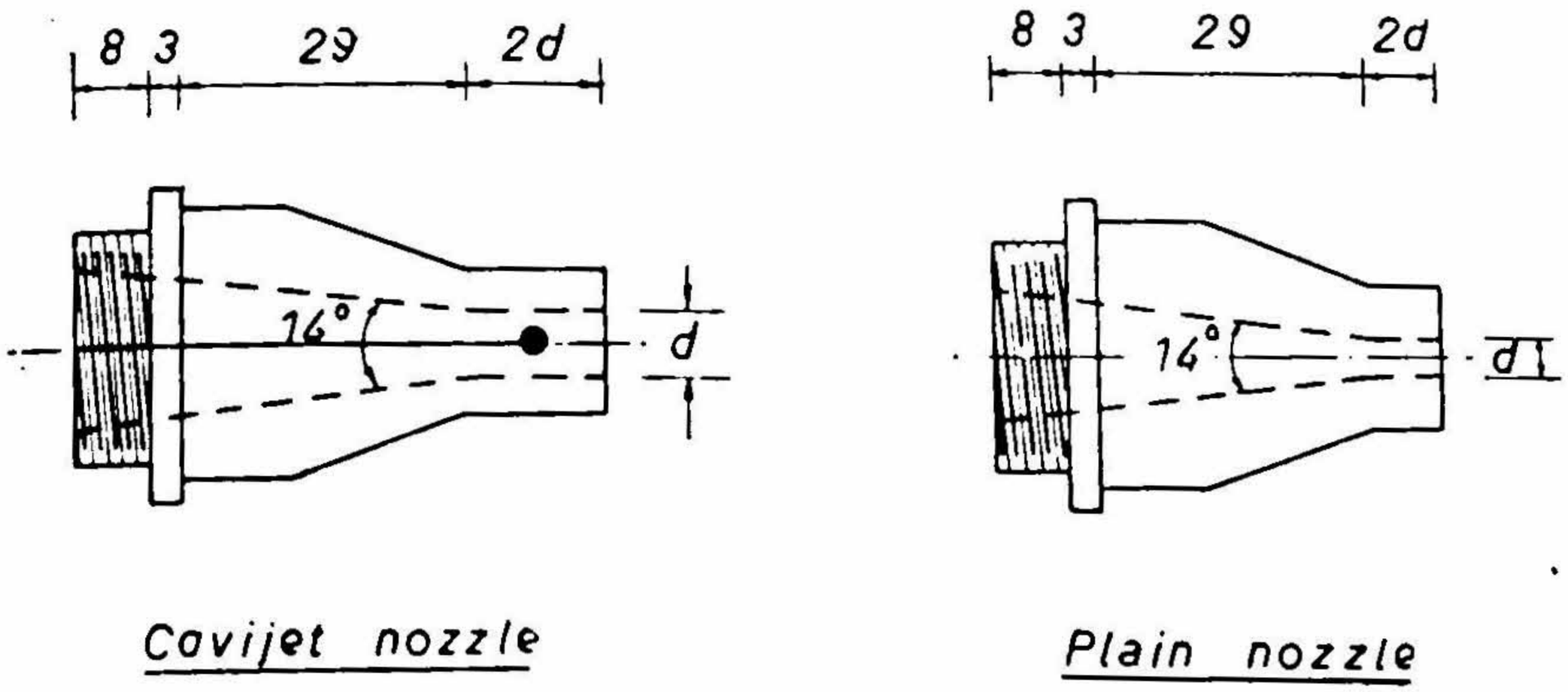

FIG. 2. Nozzle. (dimensions in mm).

50 mm × 38 mm are cut out of a 3 mm thick, commercially pure aluminium sheet The stand-off distance between the nozzle and the target can be varied from 20 to 400 mm and the jet velocity from 5 to 100 m/sec. The average velocity of the jet is calculated from the discharge which is measured using a volumetric tank.

3. Analysis and discussion

3.1. *Dimensional analysis*

The several parameters that influence erosion due to liquid jet impingement may be grouped as :

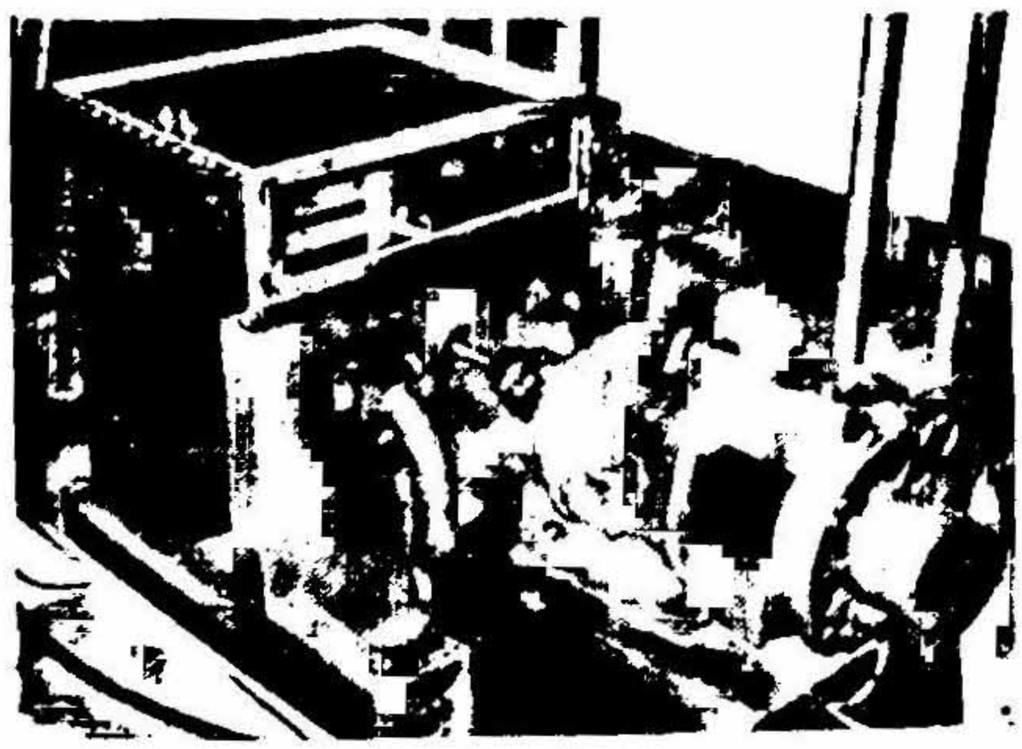

FIG. 3*a*. A view of the test rig.

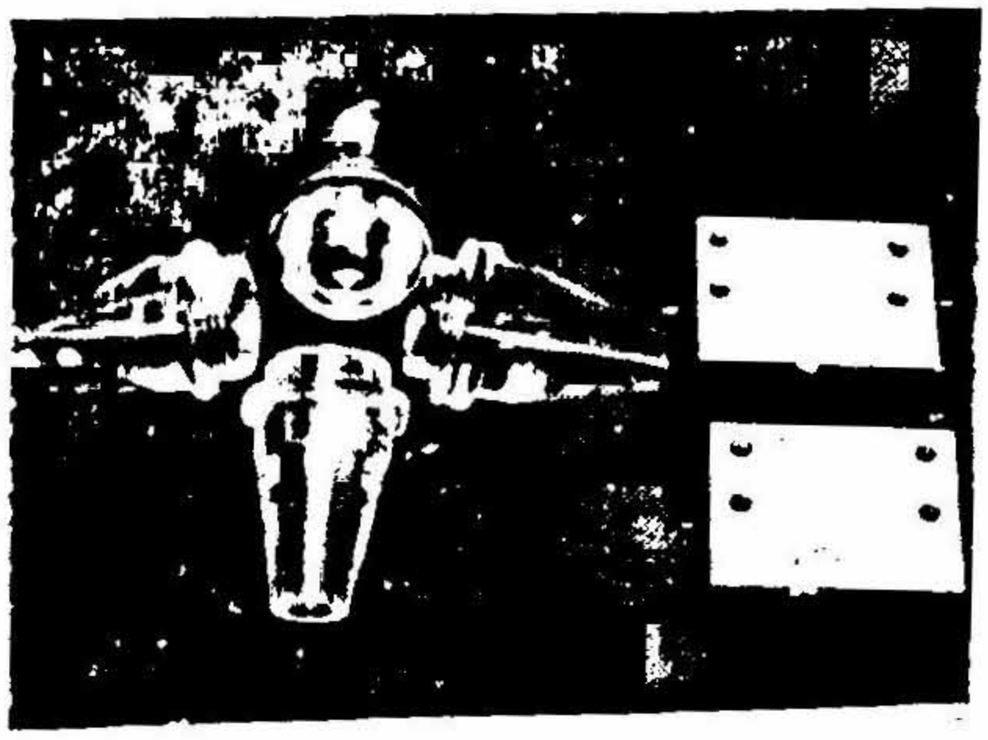

FIG. 3*b*. Nozzles and specimen.

(1) The hydrodynamic parameters—the stand-off distance of the target from the nozzle L, the test duration T, the jet velocity U_0, the tangential velocity of the target, U_T the diameter of jet D, the diameter of inducer d, the jet pressure P_i and the minimum pressure attained in the jet p_{min} for jets with cavitation inducers

(2) The frequency of impacts f and the angle of impingment θ ;

(3) The physical properties of the liquid-density e_l, acoustic velocity c_l or bulk modulus, and viscosity μ ; and

(4) The mechanical property of the target material responsible for resistance to erosion M_t, the density of the material e_t, and the acoustic velocity of the target material C_t.

By using U_0, D and e_l as the basic parameters the following dimensionless relationship is obtained :

$$\epsilon = \epsilon\left[\left(\frac{V_t}{tU_0^2D^2}\right), \left(\frac{A_e}{D^2}\right)\right]$$

$$= F\left[(L/D), (U_0t/D), (D/d), (p_i/e_l\ U_0^2), S, \theta, \left(\frac{e_t}{e_l}\right), \left(\frac{U_0}{e_l}\right), R_e, (M_t/e_lU_0^2), (U_0/e_t\right] \quad (1)$$

where $R_e = e_l\ U_eD/\mu$ is the Reynold's number and $S = tD/U_0$ is the Strouhal number.

The ratio V_t/tU_eD^2 may be slightly modified to $V_t/\pi/4D^2U_Rt$ make it a ratio of the volume loss to the volume of liquid impinging

where $U_R = (U_0^2 + U_T^2)^{1/2}$.

3.2. *Influence of stand-off distance on erosion*

The stand-off distance was varied from 20 to 240 mm and the frequency of impingement was kept constant at 33·3 Hz. Figures 4 and 5 present plots of normalized volume loss against stand-off distance for plain and cavitating jets respectively. In both the cases, the normalized erosion rate increases in the beginning, attains a peak, and then decreases as the stand-off distance is increased. Visual observations with the plain jets indicated that for maximum erosion the air content in the jet is also important. For a turbulent jet the velocity distribution across the jet is rectangular at the exit of the nozzle and becomes exponential around ten diameters of distance[11], Further ahead, the jet expands and spreads to a wider diameter. This spread decreases the impact pressure on the target and hence the erosion reduced. Figure 4 shows that the maximum erosion occurs at a stand-off distance varying from 15 to 35 diameters.

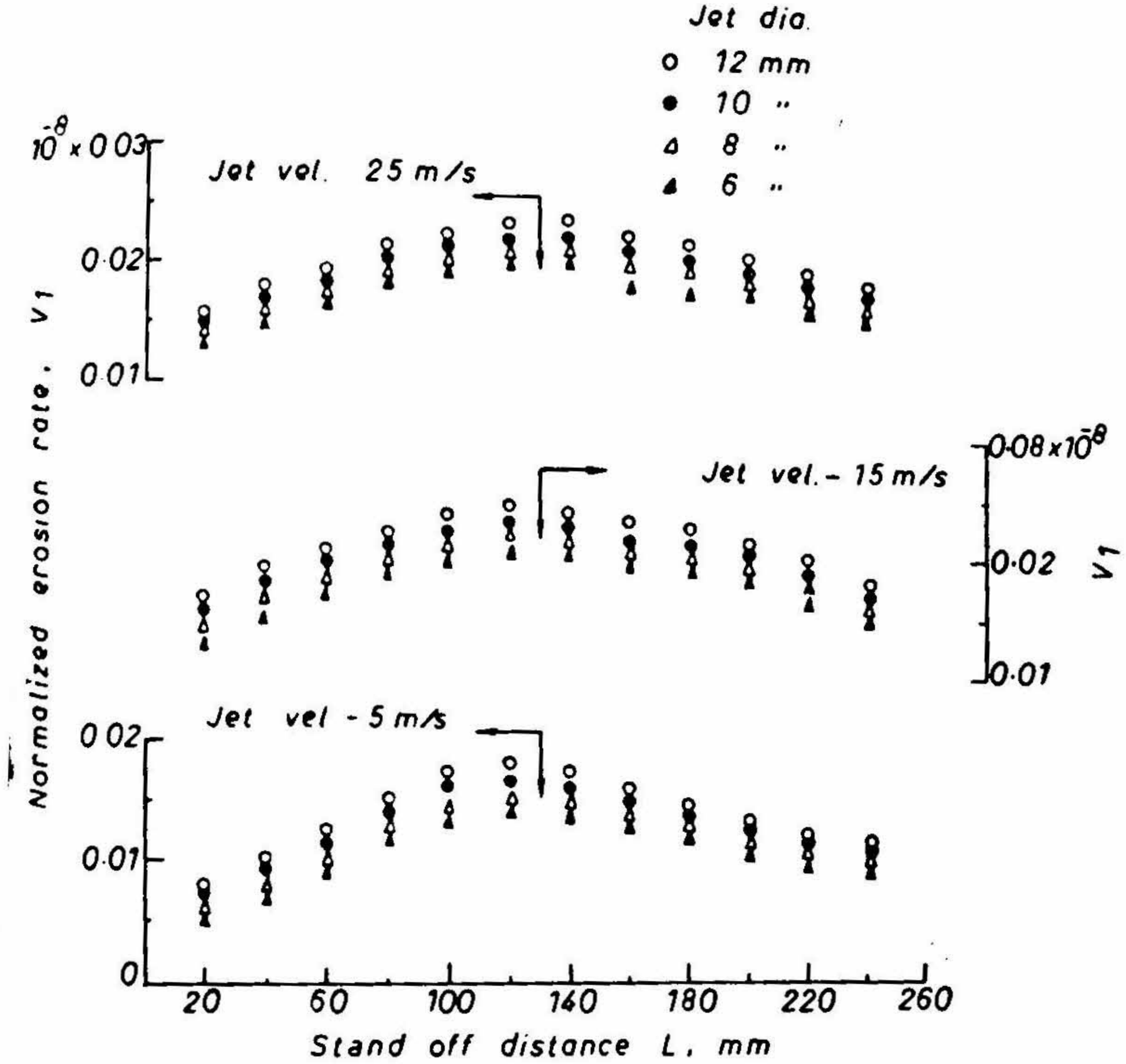

FIG. 4. Variation of normalized erosion rate with stand-off distance for plain jets.

The peak in erosion is observed in the range of 15 to 20 equivalent diameters and occurs at a larger stand-off distance than with the plain jets, which may be attributed to the effects of the inducer in the nozzle. With further increase in the stand-off distance the erosion decreases because the cavitation bubbles collapse before reaching the target. In addition, at large distances from the nozzle, the jet continues to spread rapidly and hence the impact pressures are lower.

Figures 6 and 7 show the variations of the area of erosion with stand-off distance for plain jets and cavitating jets respectively for four jet velocities. These tests are made at an impingement frequency of 50 Hz. It may be seen from fig. 6 that the increase in area of erosion with stand-off distance is approximately linear for all the plain jets. For each jet the area of erosion increases with the decrease in jet velocity.

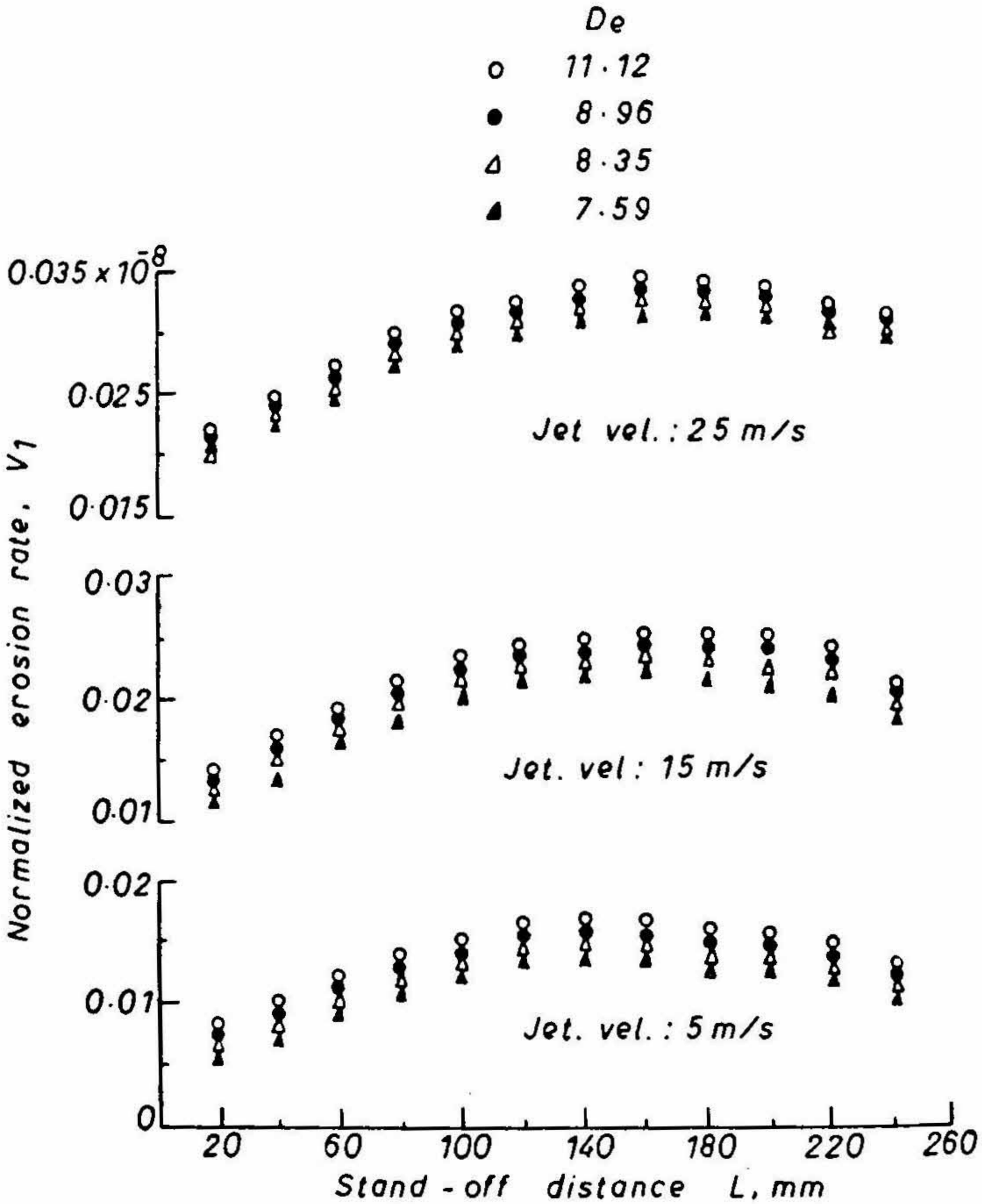

FIG. 5. Variation of normalized erosion rate with stand-off distance for cavijets.

In case of cavitating jets, the normalized area of erosion increases rapidly with stand-off distance up to about 120 mm and then remains approximately constant for larger values of stand-off distance. For cavitating jets of diameter ratio 10/5·5 and 10/6·5, with increase in jet velocity the normalized area of erosion increases. The area of erosion depends on the diameter ratio for the cavitating jets.

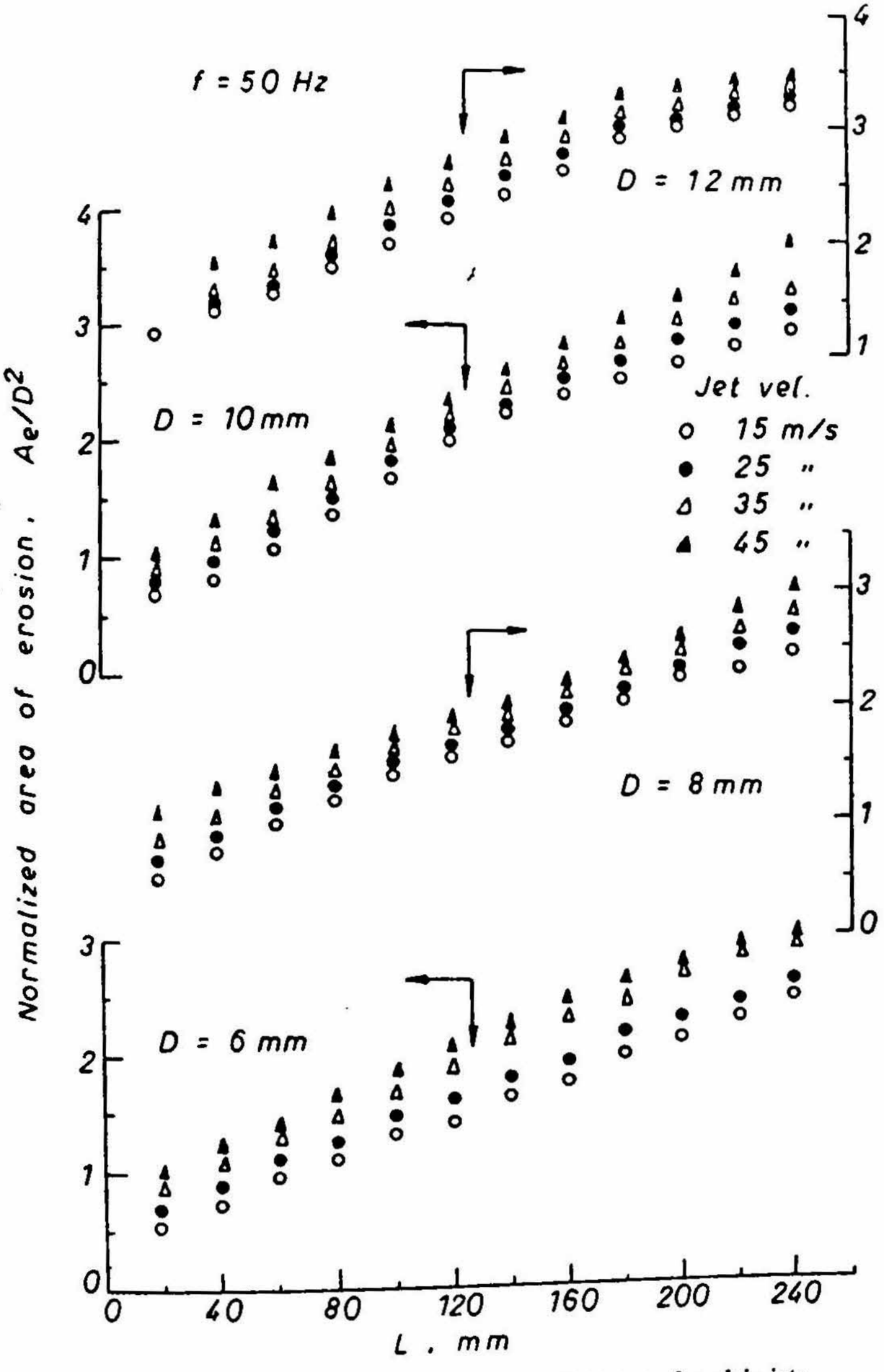

FIG. 6. Variation of area of erosion with stand-off distance for plain jets.

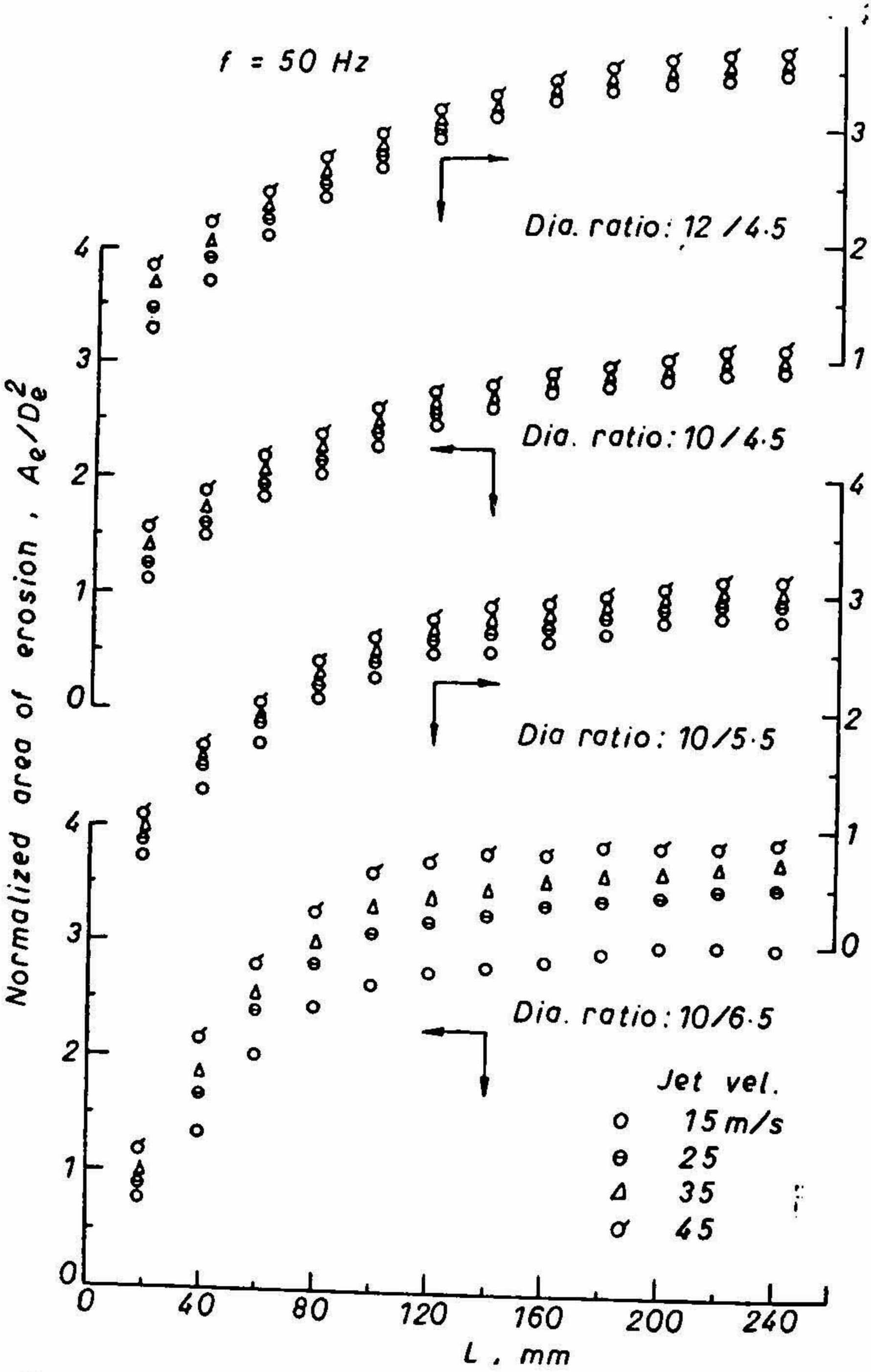

FIG. 7. Variation of area of erosion with stand-off distance for cavijets.

3.3. *Growth of jet diameter with distance from the nozzle*

Figure 8 shows the increase in jet size with distance measured from the nozzles for different plain jets. The jet size is obtained by measurements on still photographs and by using the profile gauge. The increase in ratio of jet diameter to the nozzle diameter with distance is also shown in fig. 8. Based on the spread, the jet may be divided into three distinct regions along its length: (i) the initial region, (ii) the transition region and (iii) the main region. The initial region is a potential core region where the jet size does not increase. The transition region is more clearly observed in the case of small jet diameters than in the case of large jet diameters.

In the main region the spreading rate is essentially constant for a considerable distance downstream if minor deviations due to break up of the jet are ignored.

The increase in jet size in the main region may be expressed as

$$\frac{D'}{\bar{D}} = K_1 \sqrt{\bar{L}/D'} + C_1 \text{ for } \sqrt{L/\bar{D}'} > 2{\cdot}5 \tag{2}$$

where D' is the jet width at any section distance D from the nozzle, and K_1 and C_1 are coefficients. The coefficients K_1 and C_1 are found to be 0·149 and 0·64 respectively. Up to $\sqrt{\overline{L'D'}} = 2{\cdot}5$ the jet does not spread with increase in distance.

3.4. *Effect of jet velocity on erosion*

There have been many attempts to relate the impact velocity of jets and droplets with erosion[7–9]. Though a common unified relationship has not been given between erosion rate and velocity of impact, a large increase in erosion occurred with increase in velocity. Some of the empirical relationships given[6] are

$$V_t/t = V^n \text{ and} \tag{3}$$

$$V_t/t = W(V - V_*^n) \tag{4}$$

where V_t/t is the erosion rate, W is mass of water impinging on the specimen, and V_* is the threshold velocity below which no erosion was observed. To understand the dependence of erosion on velocity, damage data were obtained with the six plain jets over the range of velocities from 5 to 45 m/s and the frequency of impingement varying from 33·3 to 100 Hz. The volume loss V_t is normalized as shown in eqn. 1 by

$$V_1 = \frac{V_t}{(\pi/4)\, t U_R D^2} \tag{5}$$

Figure 9 presents the plots of normalized erosion rate V_1 with jet velocity U_0/C_t for the frequencies of impingement of 33·3, 66·6, and 100 Hz. The inset in the same figure shows the average variations of V_1 with U_0/C_t at the five different impingement frequencies for the jet size $D = 8$ mm.

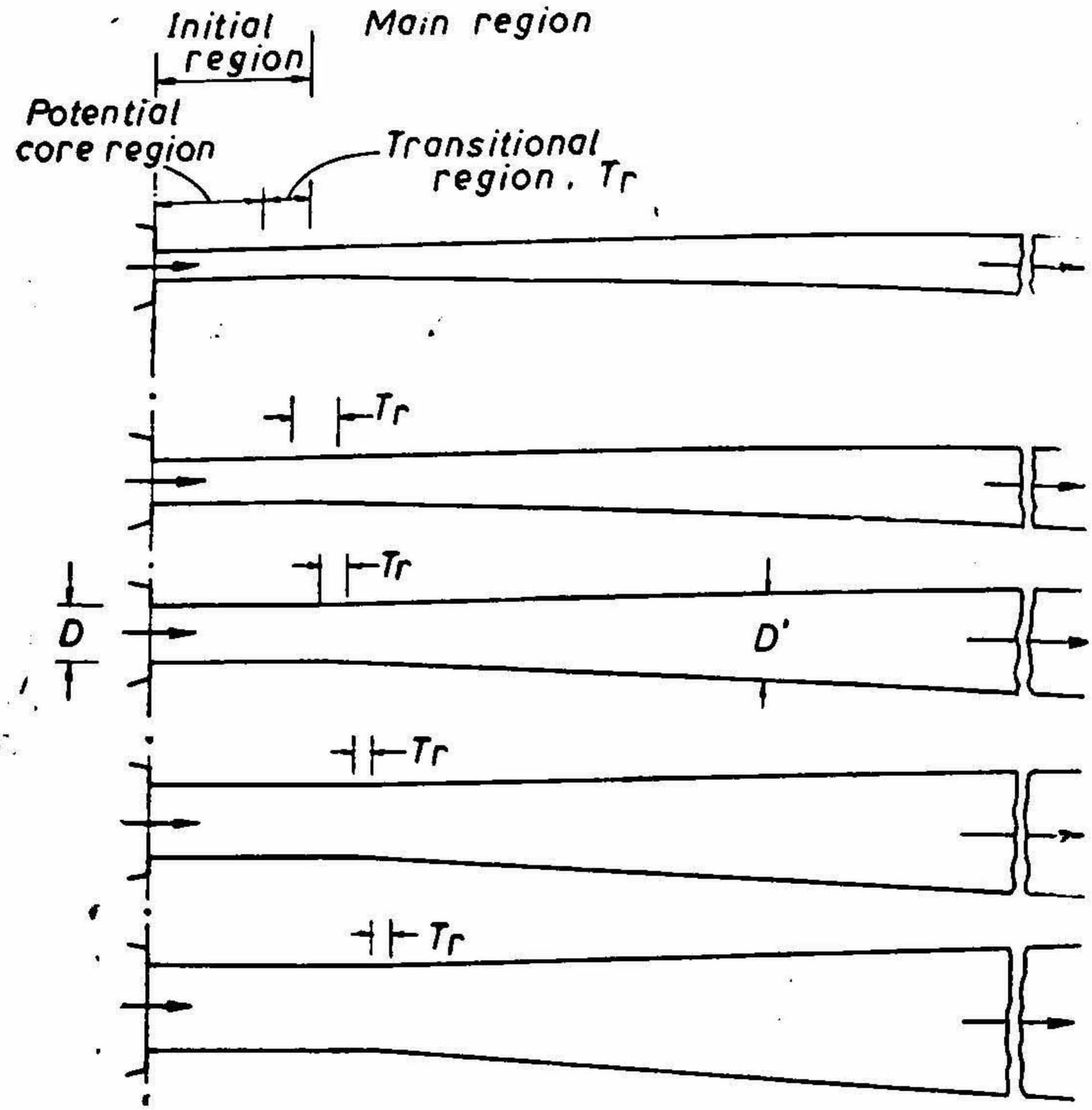

FIG. 8. Growth diameter of jet with stand-off distance.

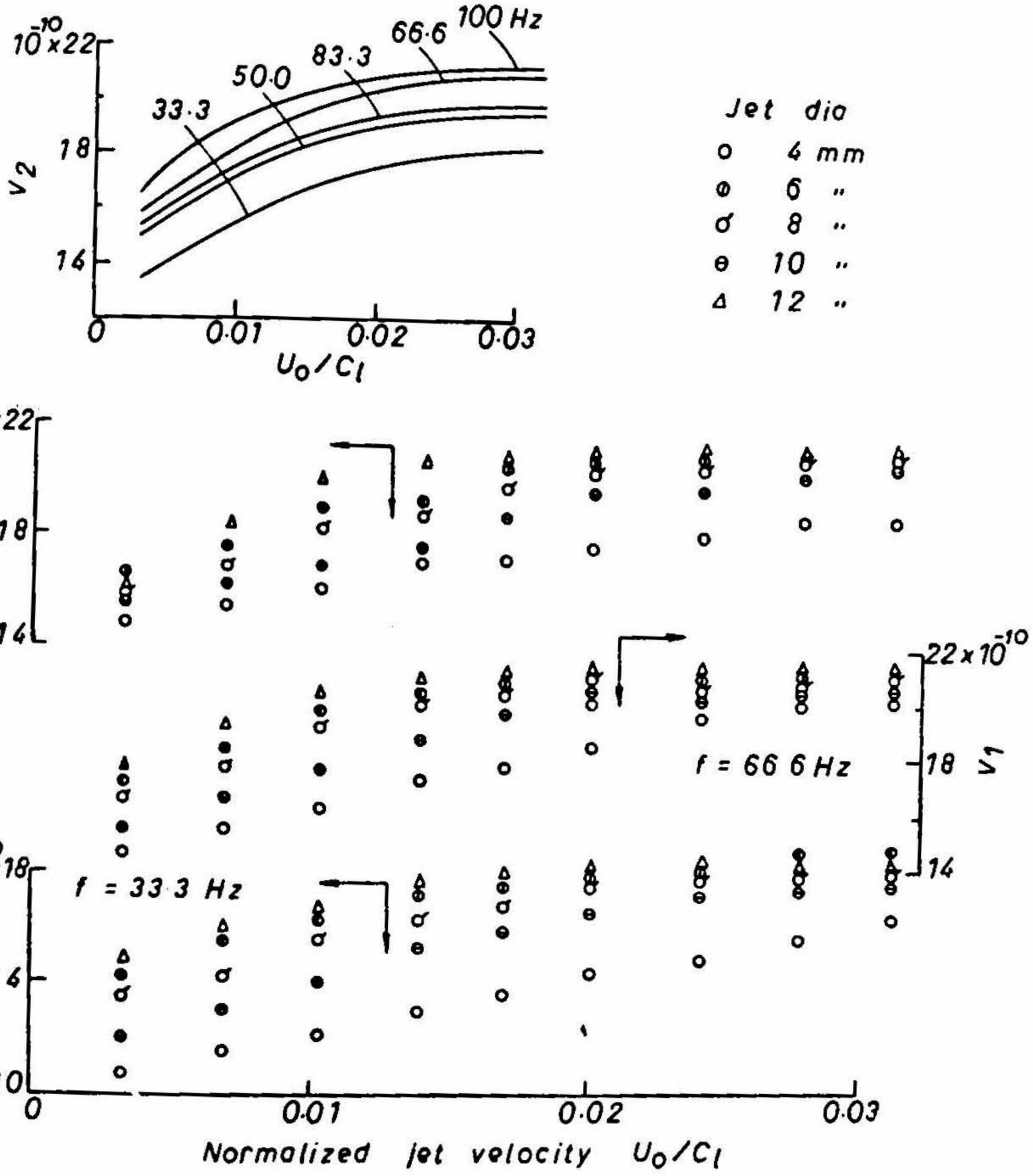

FIG. 9. Influence of jet velocity on normalized erosion rate.

Figure 10 presents the variation of rationalized volume loss $V_r = (V_1/t)/V_p/t_p)$ with jet velocity U_0/C_l, where V_p indicates the volume loss at peak erosion rate. The quantity V_r is the ratio of the the volume loss rate at the end of 5 hr to the peak volume loss rate. The peak in volume loss rate occurred after a definite interval of test duration in the case of plain jets, unlike that for cavitating jets shown in fig. 5, where a continuously decreasing rate is observed. The small inset in the figure gives the average variations of V_r with U_0/C_l which shows again that this type of non-dimensionalization also does not fully take care of the impingement frequency effects.

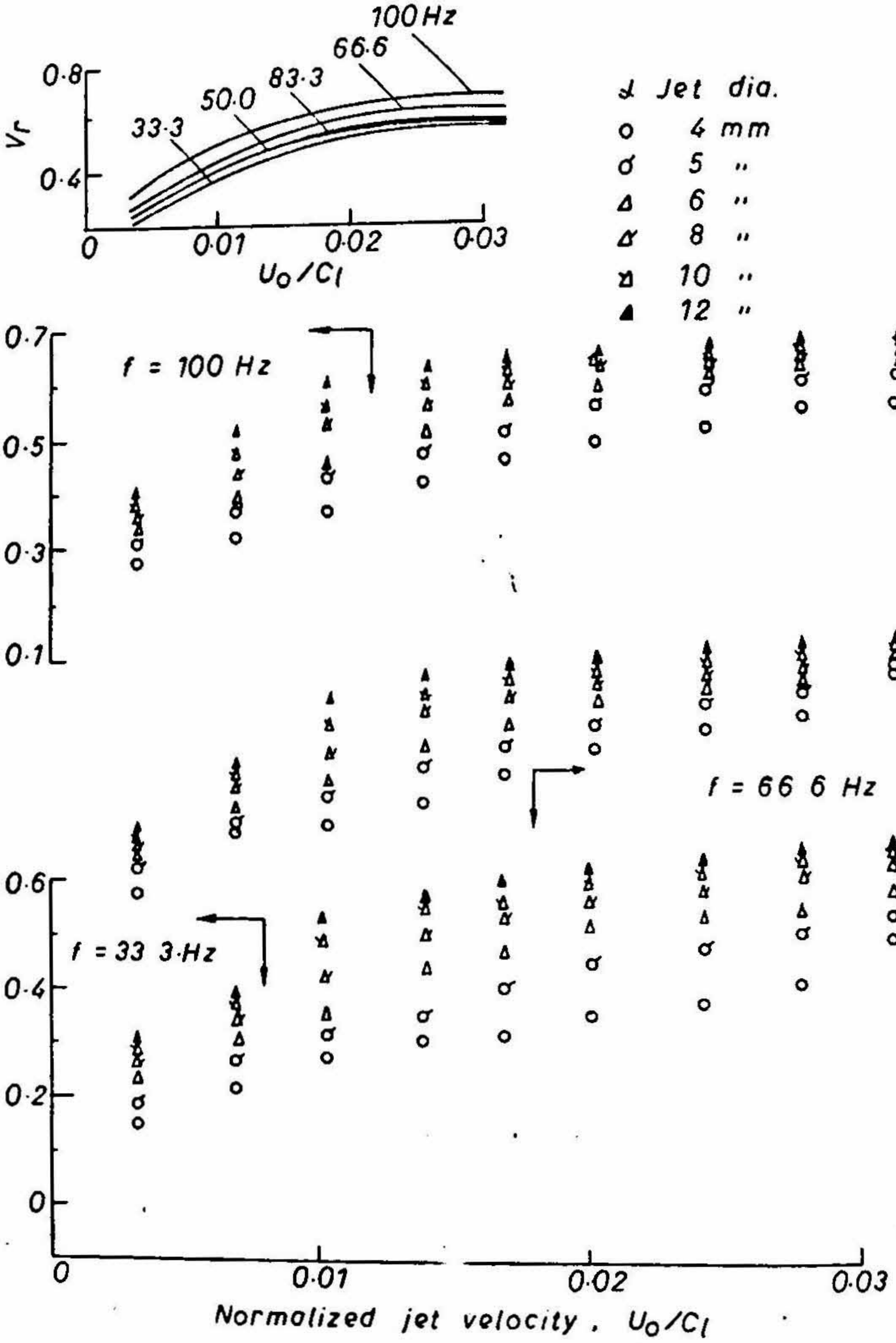

FIG. 10. Influence of jet velocity on rationalised volume loss.

The quantity V_1 may be considered as the ratio of volume loss to the volume of liquid impinging. From fig. 10, it may be seen that this ratio approaches a constant value as the jet velocity increases. The same trend is also seen in fig. 10.

Similar attempts using the data for cavitating jets, however, did not result in meaningful plots. Hence, a cavitation parameter K_0' was defined as

$$K_0' = (p_0 - p_v)/(1/2\, e_l U_0^2) \tag{6}$$

In the present study the pressure p_{min} at a point on the disturbance (cavitation source) in the nozzle where the velocity is maximum is used in place of p_0.[6] Hence the cavitation number in eqn. 9 is redefined for the present analysis as

$$K_0 = (p_{min} - p_v)/(1/2\, e_l U_0^2) \tag{7}$$

Figure 11 shows the variation of normalized erosion rate with cavitation number for three different impingement frequencies. The inset in the figure gives a plot of the average variations of V_1 with K_0 for six impingement frequencies. In the plots two zones could be identified ; one shows a rapid fall in erosion with increase in K_0, and the second, where a gradual decrease in volume loss rate is conspicuous, is perhaps due to the cavitation effects becoming less significant.

3.5. *Influence of frequency of impingement on erosion*

A number of investiagtors[7–9] have reported the dependence of erosion on the impingement frequency of droplets and jets. The number of impacts were varied either by injecting the liquid on moving specimens or by having intermittent or pulsed jets. Hancox and Brunton[8] reported that there was a threshold frequency below which no apparent change in surface structure occurred. With copper and aluminum targets an initial quiescent period during which no detectable damage occurred was observed.

In the present investigations keeping all the other parameters constant, the effect of variation in frequency of impacts on erosion is studied for four jet velocities and nine different jets. The frequency of impingement f is normalized considering the threshold frequency I_0 which is defined as the number of impacts necessary to initiate damage on the material at a given jet velocity[11]. The threshold values are obtained by extending the linear portions of the volume loss plots to the x-axis. Figures 12 and 13 present plots of normalized quantities for plain jets and cavitating jets respectively. These indicate a unified variation of normalized erosion rate with normalized frequency of impingement. In the case of 4 mm diameter plain jet, the increase in normalized erosion rate with increasing frequency is faster than the same for jets of 6, 8, 10 and 12 mm diameters. This shows that small diameter jets are more efficient than large diameter jets considering the quantity of liquid impinging. Figure 13 shows that for cavitating jets the erosion rate has a uniform increase with increase in frequency for jets of 7·59 and 8·35 mm equivalent diameter. However, for jets with $D_e = 8{\cdot}96$ and 11·16 mm the erosion increases faster for $f/I_0 > 8$, than the same at lower values of f/I_0.

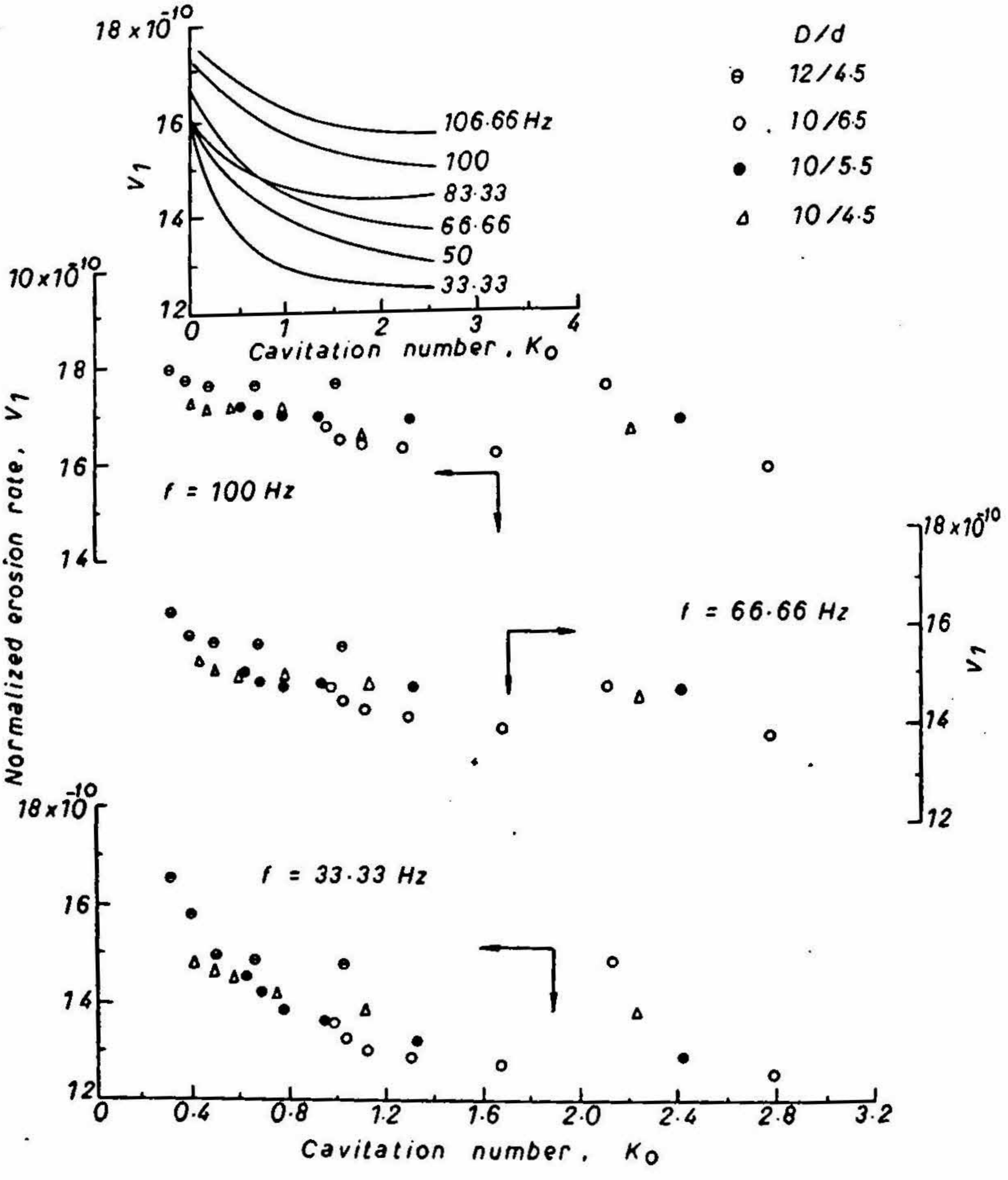

FIG. 11. Variation of normalized erosion rate with cavitation number.

Figure 14 shows the logarithmic variation of normalized erosion rate with the normalized frequency of impingement for the five plain jets and four cavitating jets. The average trend of the experimental points may be described by the relationship :

$$V_1 = K_2(f/I_0)^n \tag{8}$$

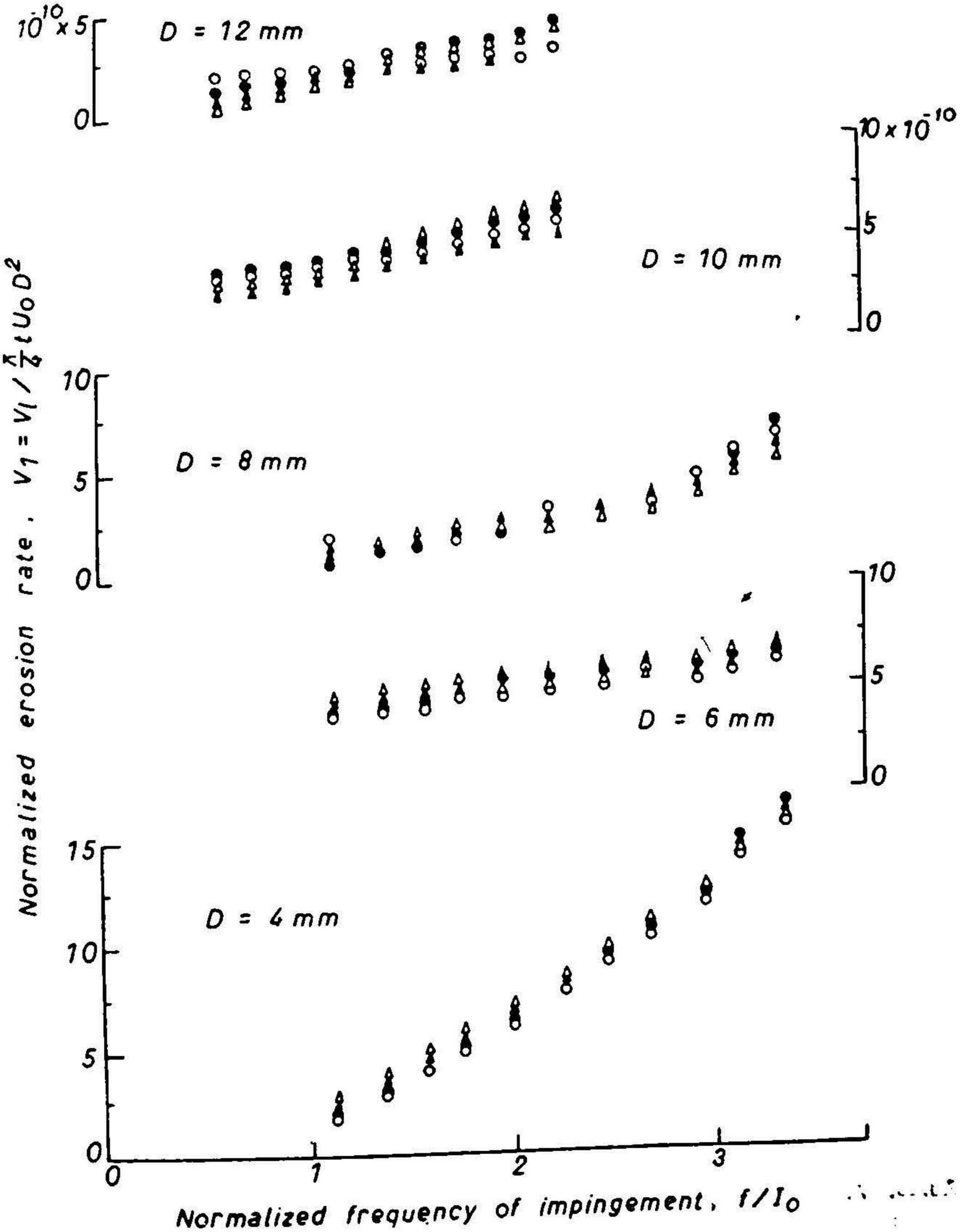

FIG. 12. Variation of normalized erosion rate with normalizod frequency of impingement plainjets.

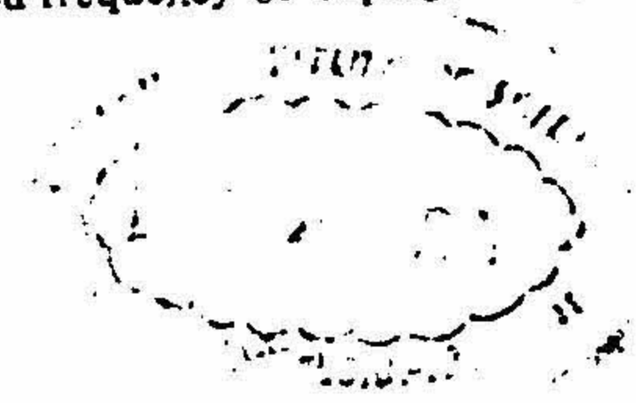

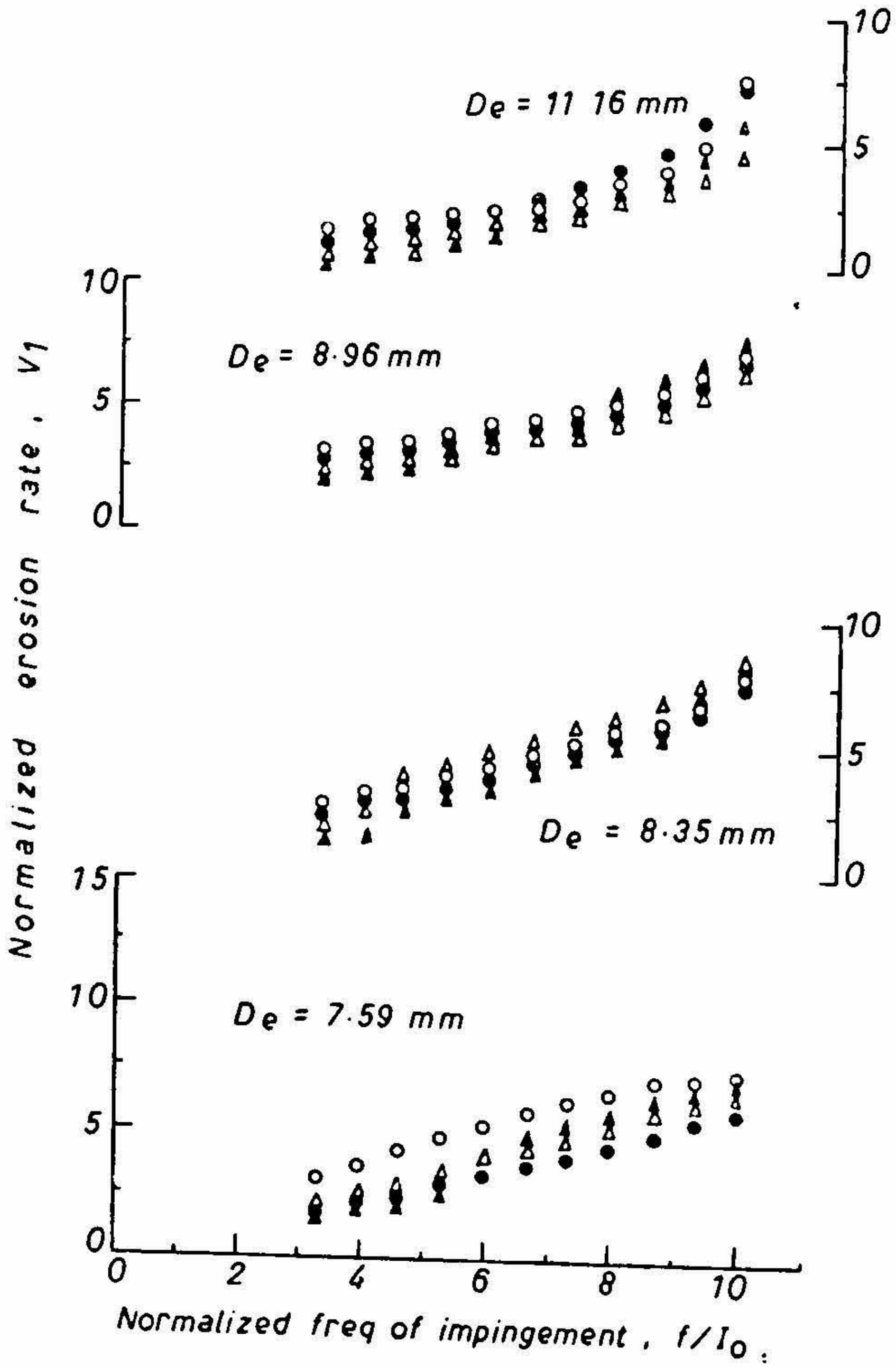

FIG. 13. Variation of normalized erosion rate with normalized frequency of impingement for cavijets.

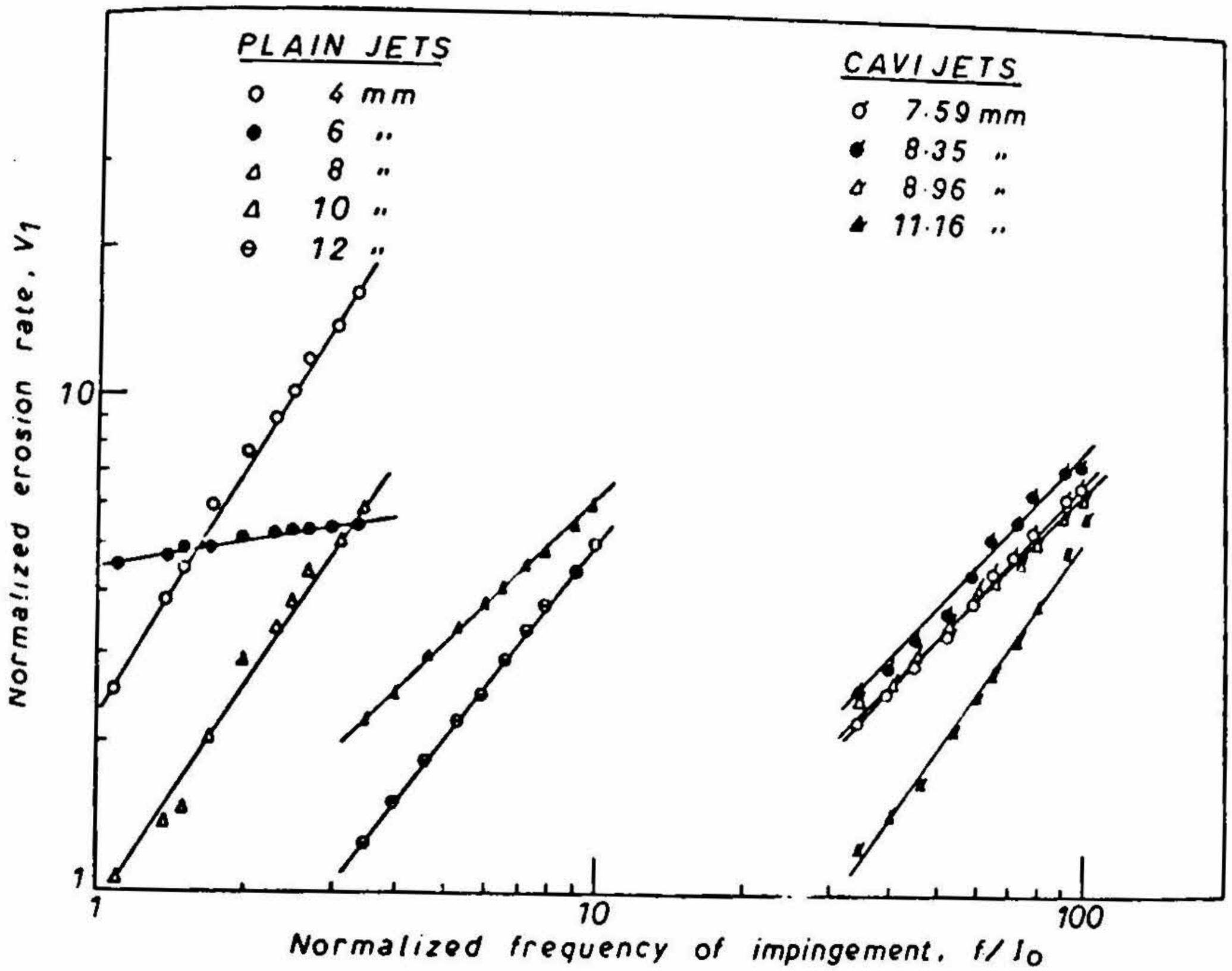

FIG. 14. Logarithmic variation of normalized erosion rate with normalized frequency of impingement.

where V_1 is the normalized erosion rate considering the volume of liquid impinging, Ke is a coefficient and n is an exponent. The exponent n is found to vary from 0·16 to 1·75 for plain jets as the diameter increased from 4 to 12 mm and from 1·02 to 1·47 for cavitating jets as the equivalent jet diameter increased from 7·59 to 11·16 mm. When the dimensional quantity volume loss V_t is plotted against the frequency of impingement f, it is found that V_t varied with 4th and 9th power of f as the diameter of jet increased.

3.6. *Influence of the angle of impingement on erosion*

The angle of impingement plays a significant role in the case of erosion of turbine blades and aircraft. In the present experiments the angle subtended by the resultant velocity with the target specimen varied from 15 to 65°. The tangential velocity of the target specimen was varied from 15 to 60 m/s. The erosion data were obtained for a total of 5 hr for each of the specimen. Figure 15 shows a plot of normalized erosion rate

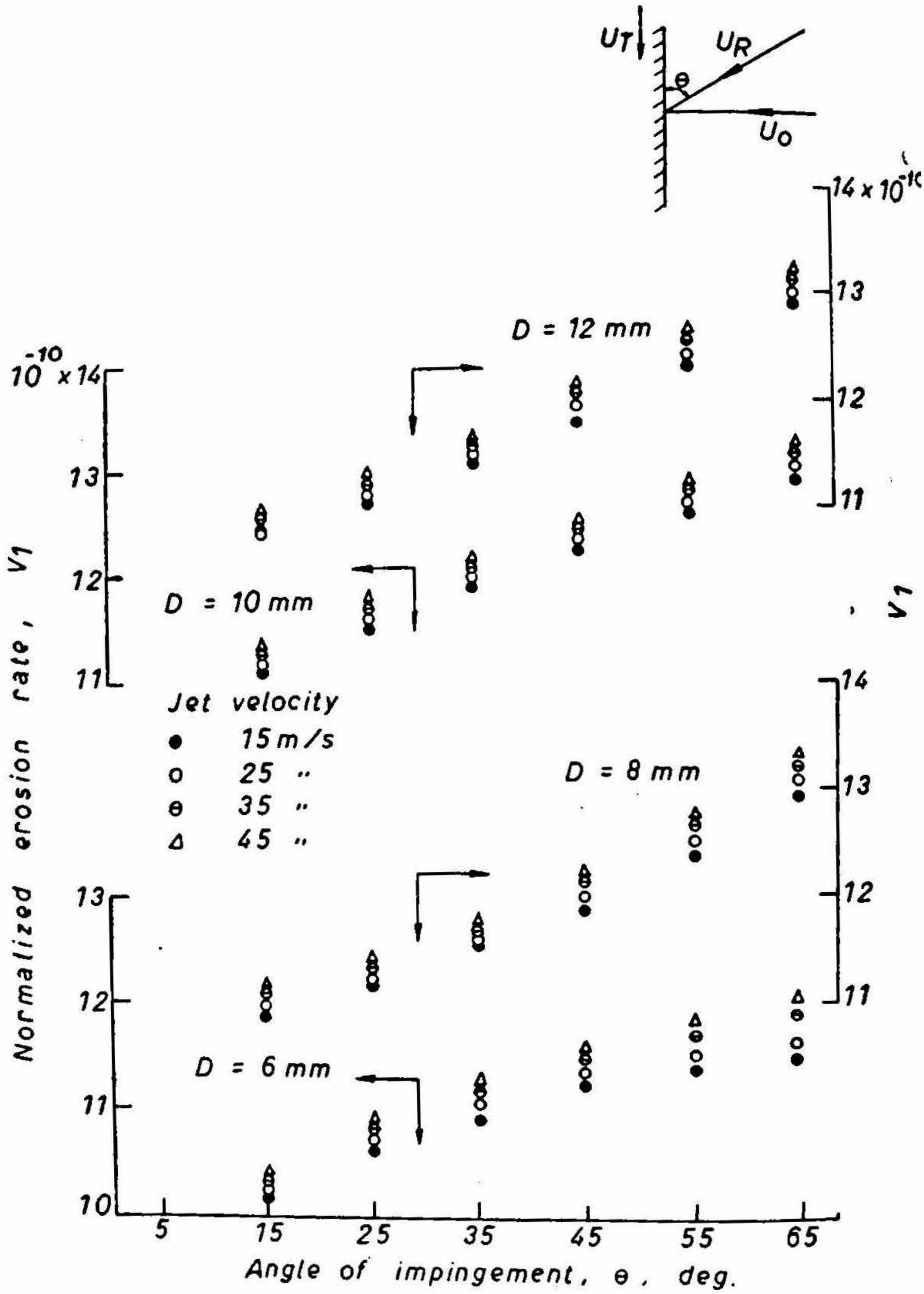

FIG. 15. Variation of normalized erosion rate with angle of impingement for plainjets.

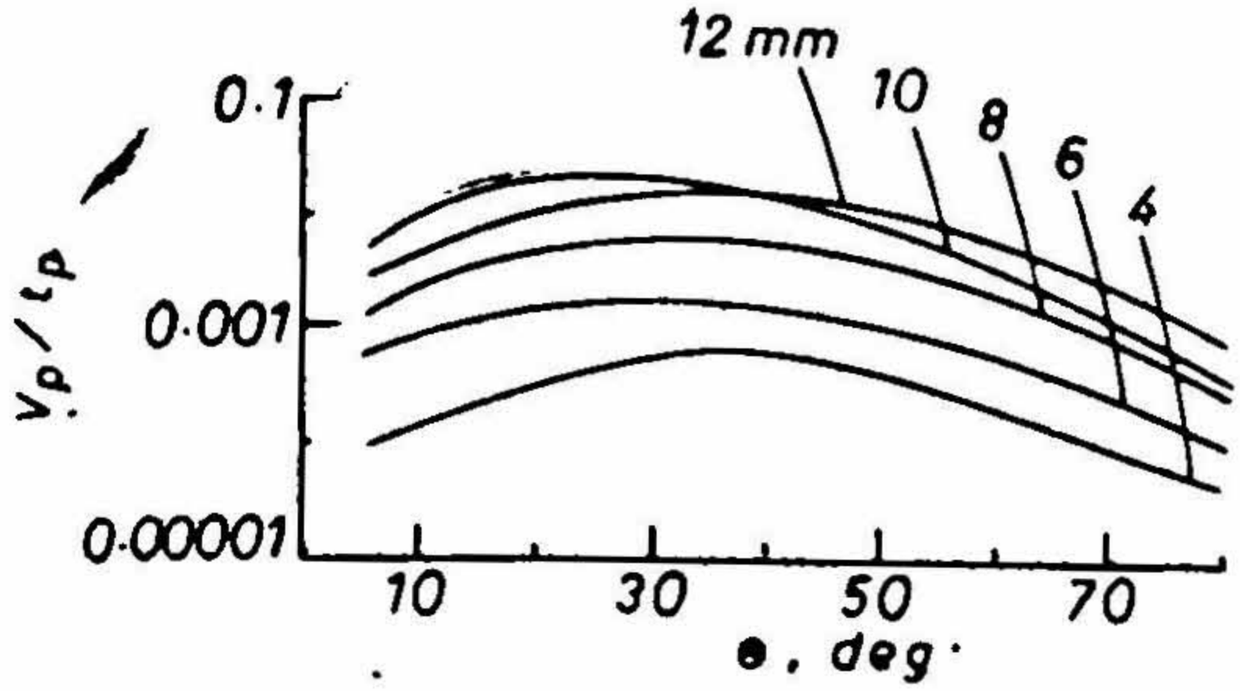

FIG. 16.

with the angle of impingement. The erosion rate increases with increase in the angle of impingement. A plot of the peak volume loss rate *vs* angle of impingement, presented as an inset in fig. 16, indicates that the peak erosion rate attains a maximum value between 25 to 40° for various jet diameters.

3.7. *Influence of test time on erosion*

The importance of test time, which has received much attention, is in the evaluation of the resistance of materials to erosion. Several investigators[9–18] have reported that the characteristic erosion rate-time curves of damage resulting form cavitation or impingement could be described in terms of four zones as (1) an incubation zone, (2) an accumulation zone, (3) an attenuation zone, and (4) a steady-state zone. In the present investigation the erosion rate-time variation of aluminium target specimen exposed to the impingement of four different cavitating jets was studied (fig. 17). The weight loss measurements were taken at intervals of 20 min over a total period of 5 hr. The trend of variation in fig. 17 is similar to that observed in the case of plain jet impingement[6, 11] and the scatter of experimental points is slightly less. Also the incubation and the accumulation zones are not significantly shown and the erosion rate is higher than with plain jets. In the attenuation zone, a rapidly decreasing rate of erosion is observed with increase in test time and, further, the erosion rate becomes approximately constant.

Observations of the eroded test specimen at several test durations indicated that initially the material was removed uniformly from the surface. During the attenuation zone a gradual development of large craters with increase in the area of erosion was observed. The trapping of liquid and cavitation bubbles on the eroded surface caused cushioning and screening effects that resulted in the attenuation of erosion. During this test time, the work hardening effects on the eroded area may also have contributed to the decrease in erosion rate.

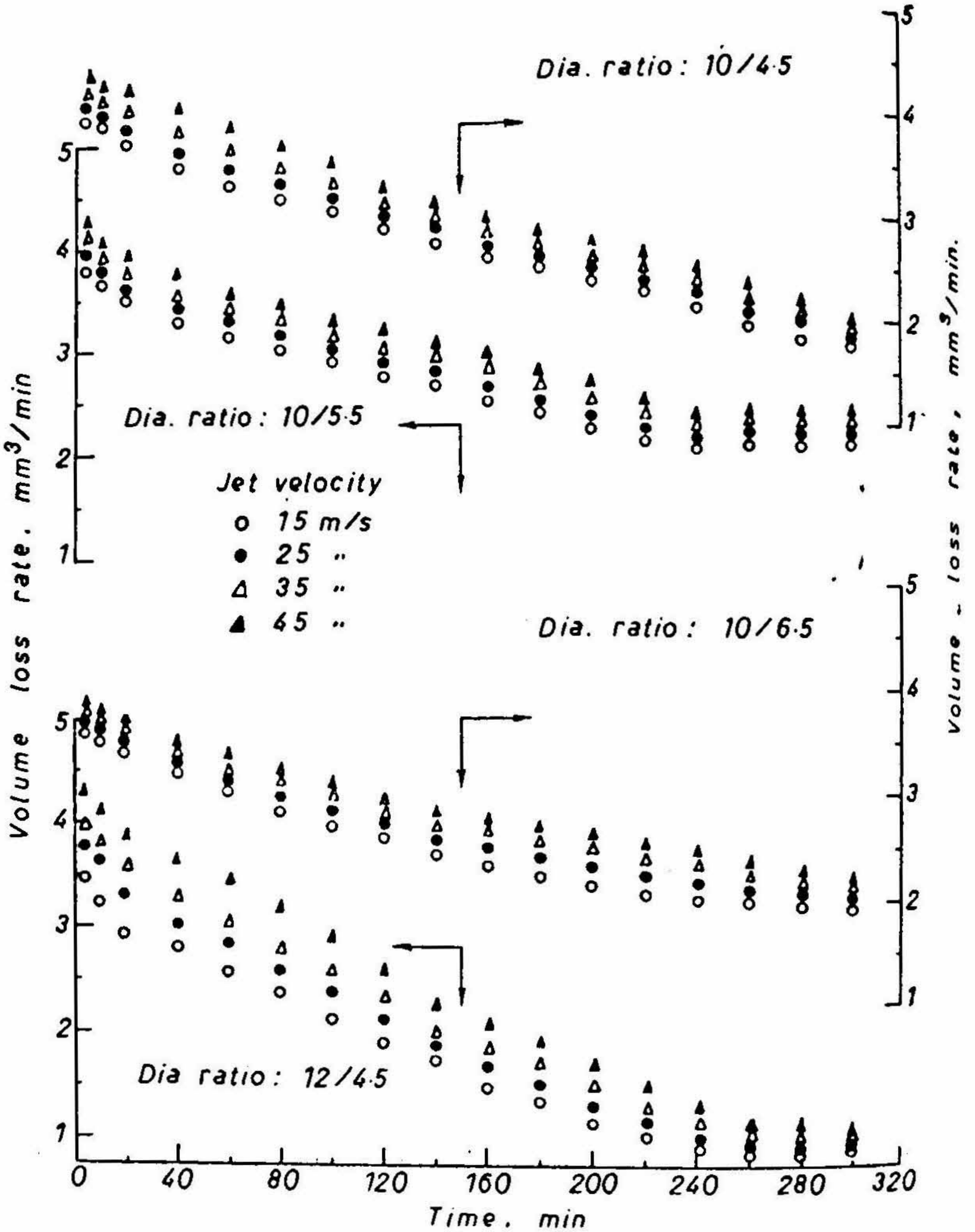

FIG. 17. Volume loss rate-time curves for cavijets (cavitating jets).

Heymann[9] presented a statistical model taking material response as a criterion in the prediction of erosion rate with rest time for varying hydrodynamic conditions. Hoff and Langbein[1] presented an equation for the erosion rate as

$$I = 1 - \exp(-t_{max}/t) \tag{9}$$

where I is the ratio of erosion rate with erosion at peak (relative erosion rate), t_{max} is the intercepted portion on the time axis from the linear portion of the erosion time curve, and t is the total test time. Thiruvengadam[8,18] proposed a theory of erosion based on the 'accumulation' and 'attenuation' of energies of impacts from microjets and shock waves. The intensity of erosion was defined as the power absorbed by a unit area of the eroded material. Figure 19 presents the variation of I against the non-dimensional test time for the erosion resulting from the cavijet of diameter ratio 10/5·5 at four different jet velocities. Theoretical variation of I with τ was obtained by using the following equation of the theory of erosion :

$$I = \frac{[e/(e-1)]\ (\eta)}{\left[1 + \frac{1\cdot 5a}{(e-1)} \int_1^{\tau} \frac{e}{e-1}\ (\eta)\, d\tau\right]^{2/a}} \tag{10}$$

where $\eta = f(\tau) = 1 - \exp(-\tau^{a})$ (Weibull distribution), $e = 2\cdot 72$, and a is dependent on U_0 as defined below.

The variation of I with a (for values of $a = 0\cdot 14$, $0\cdot 18$, $0\cdot 26$ and $0\cdot 3$) is also presented in fig. 18. In the present investigations, the exponent a in the distribution function is dependent on the jet velocity U_0 for a particular jet pressure and target material. The dependence of a on U_0 may be expressed as

$$a = p \log U_0 + Q. \tag{11}$$

The values of P and Q for the three different frequencies of impingement studied are given in table I. The derivation of eqn. (14) was based on the assumption that the

Table I

Values of P and Q for three different frequencies of impingement

f, Hz	P	Q
33·3	— 2·80	0·38
66·6	—11·92	0·13
100	—11·92	0·11

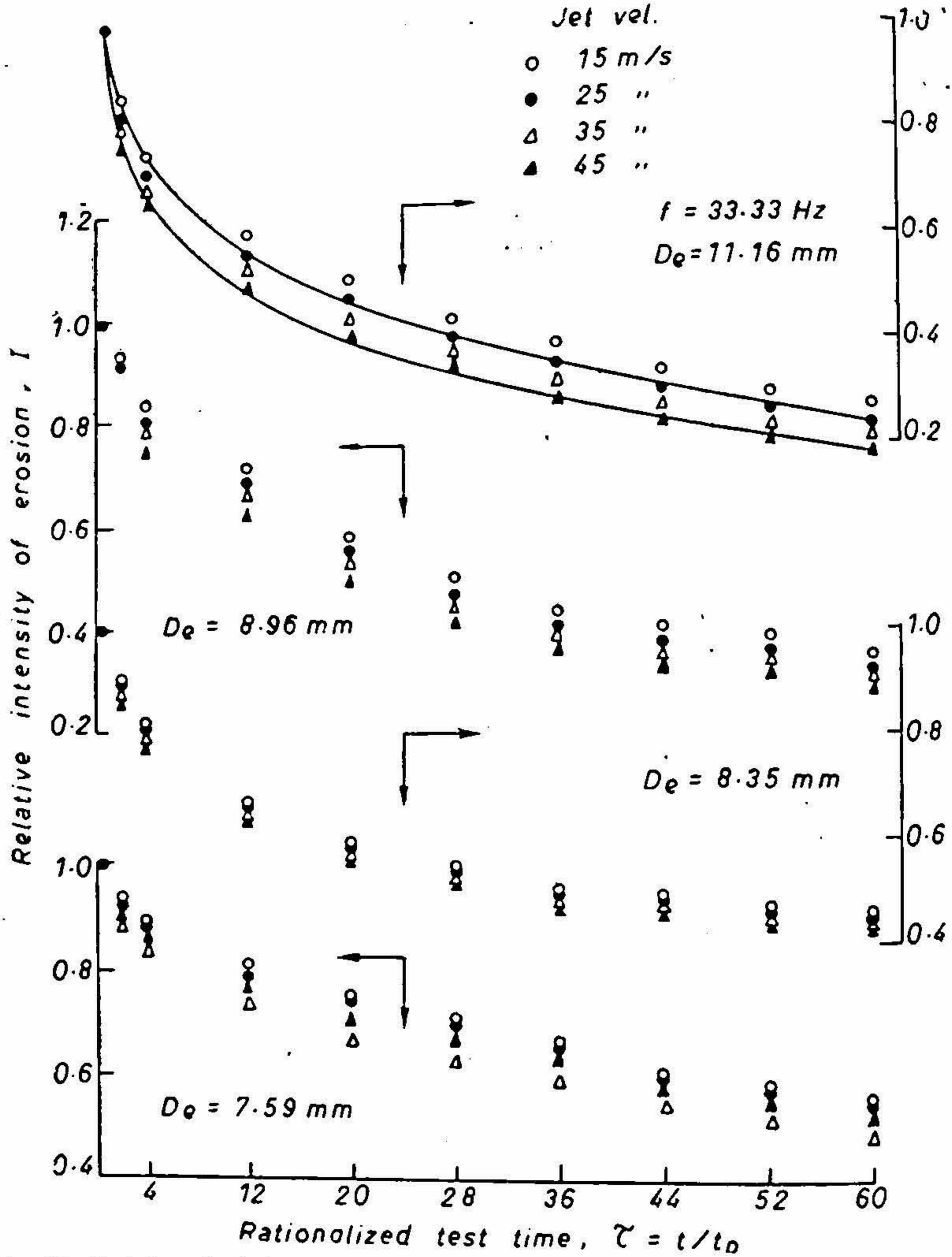

FIG. 18. Variation of relative intensity of erosion with rationalized test time.

material removal takes place because of fatigue. However, the entire material removal cannot be attributed to a fatigue process alone. Several other phenomena, like the stress concentration, shear, plastic deformation, and flow, as well as the roughness caused on the target, contribute to the total erosion.

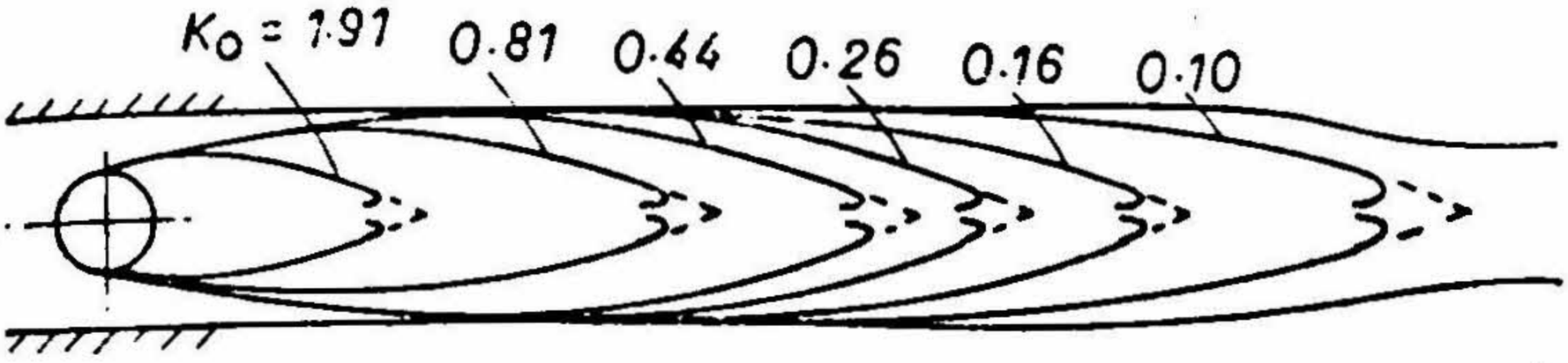

FIG. 19. Cavity shapes from visual observations.

3.8. *Shape and characteristic features of the cavitating jets*

Visual observation of the cavity are made keeping the flow velocity constant. The formation of a steady cavity was noticed in the velocity range of 5 to 30 m/sec for different nozzles. The cavities are of the type shown in fig. 19, and with increase in jet velocity the longitudinal oscillations of the cavity are found to increase. The cavity had a blunt end with a tail of bubbles which were carried away by the jet. With further increase in velocity beyond 15 to 20 m/sec, transverse oscillations of the cavity and noise are noticed. Also, the cavity length fluctuated between its maximum and minimum values at higher velocities. Beyond a velocity of 30 to 35 m/sec, the jet was in a fully turbulent condition and it was not possible to ascertain the length of cavity precisely.

The length and width of cavity were determined by taking still photographs of the cavity at different velocities. Figure 19 shows that with increase in jet velocity (decrease in cavitation number) the cavity length increases. Also, the maximum width of cavity increases with increase in jet velocity. Further, the jet size increases to a maximum and then decreases as the distance from the nozzle increases. This initial increase and then decrease in size is due to the cavity formed immediately behind the inducer. Further downstream, the jet again increases in size due to the entrainment of the surrounding atmospheric air. The jet diameter attains a minimum immediately downstream of the section where the cavity closes.

Figure 20 presents a plot of the normalized length of cavity with cavitation number. The length of cavity is normalized with the diameter of the inducer. With increase in cavitation number the normalized length of cavity decreases repidly for all the cavitating jets up to a cavitation number of about 0·7. Further, the decrease in cavity length is gradual. Similar trends were reported by other investigators in cavitation studies using venturi and rotating disc equipment[6]. The variation of the normalized maximum width of cavity b'/d with cavitation number is presented in fig. 20. For all the cavitating jets, the maximum width of cavity decreases uniformly with increasing cavitation number. The scatter in the experimental data on cavity width may be attributed to the influence of transverse oscillations of the cavity on the measurements.

Figure 21 presents a plot of the normalized erosion rate $V_1 = (V_1/\pi/4\ D_e^2\ U_0 t)$ with normalized length of cavity L'/d. It may be seen that with increase in length of cavity the erosion rate increases and attains approximately a constant value for a jet diameter. The area of erosion increases mildly up to a length of cavity L'/d equal to 9 (approximately) and then increases rapidly with further increase in length of cavity.

4. Regression analysis

A detailed regression analysis was carried out for the erosion data obtained experimentally for plain jets with the variation of test time, jet velocity, frequency of impingement and jet diameter. The data was non-dimensionalised and computations were carried out using the DEC-1090 computer. The empirical relation used to correlate erosion data with impact velocity is of the form

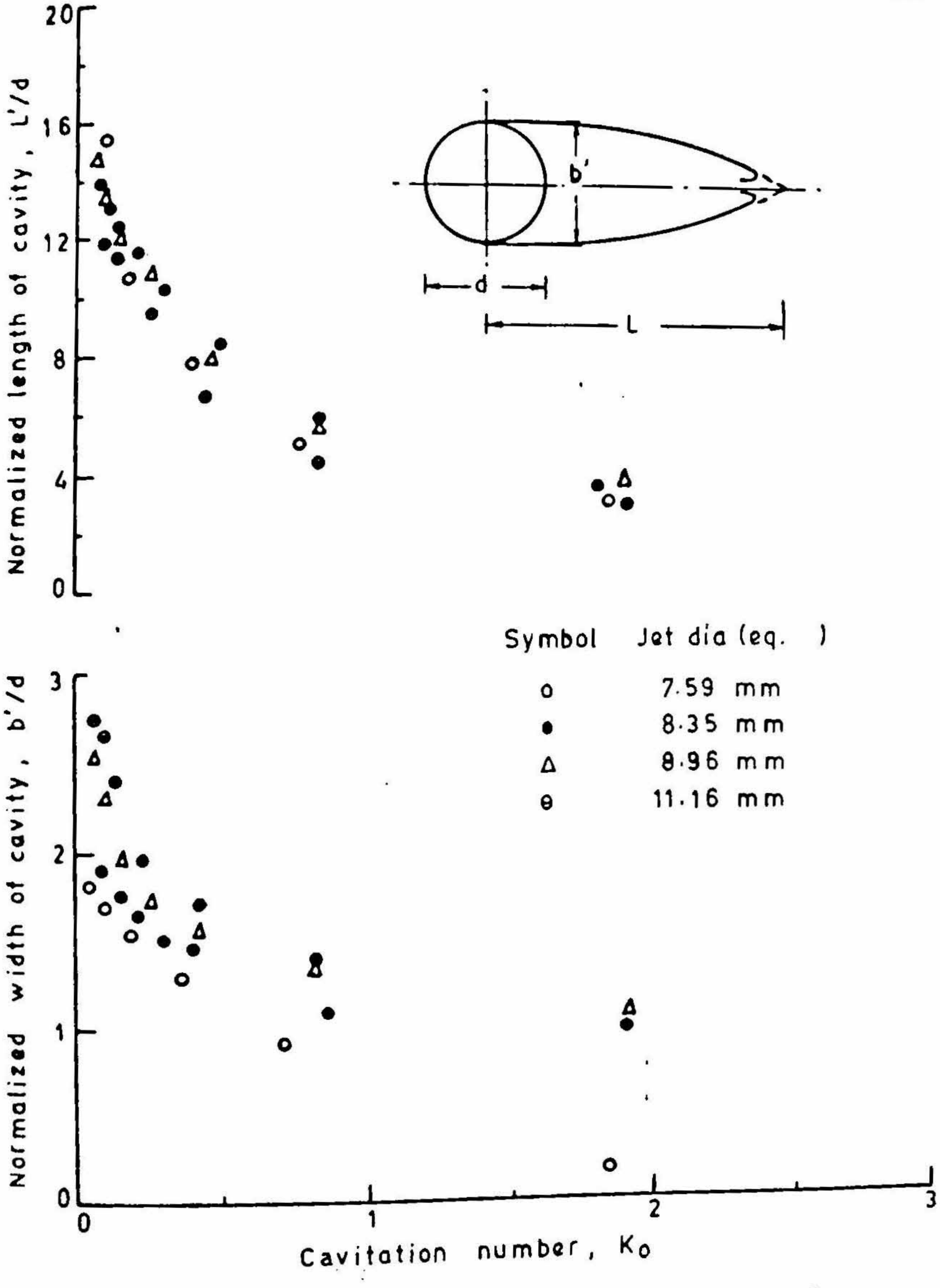

FIG. 20. Relation between normalized length and width of cavity with cavitation number.

$$\left[\frac{V_1}{D^3}\right] = A\left[\frac{U_0}{U_c}\right]^m \text{ where } U_c \text{ is the threshold velocity.} \quad (12)$$

It is seen from the analysis that the value of the exponent m varied from 0·38 to 0·66 and the constant A varied from 0·088 to 1·19. Figure 22(a) shows the variation of the exponent m with the nozzle diameter. As the nozzle size increases the exponent of (U_0/U_c) decreases. Similar exponents are oberved in case of cavitation erosion tests with rotating disc and venturi[6].

A multiple regression was also carried out to study the effects of test time, frequency and velocity on erosion. The relationship used for this analysis was of the form

$$\left[\frac{V_1}{D^3}\right] = B\left[\frac{V_0 t}{D}\right]^r \left[\frac{fD}{U_0}\right]^s \left[\frac{U_0}{U_c}\right]^t \quad (13)$$

In the analysis the values of B varied from 0·0028 to 0·0045, r from 0·25 to 0·38, s from 0·53 to 0·78 and t from 0·69 to 0·93. Figure 22 (b) shows the plots of the exponents r, s and t against nozzle diameters. The figure shows that smaller jets possess a higher cutting capacity than larger jets.

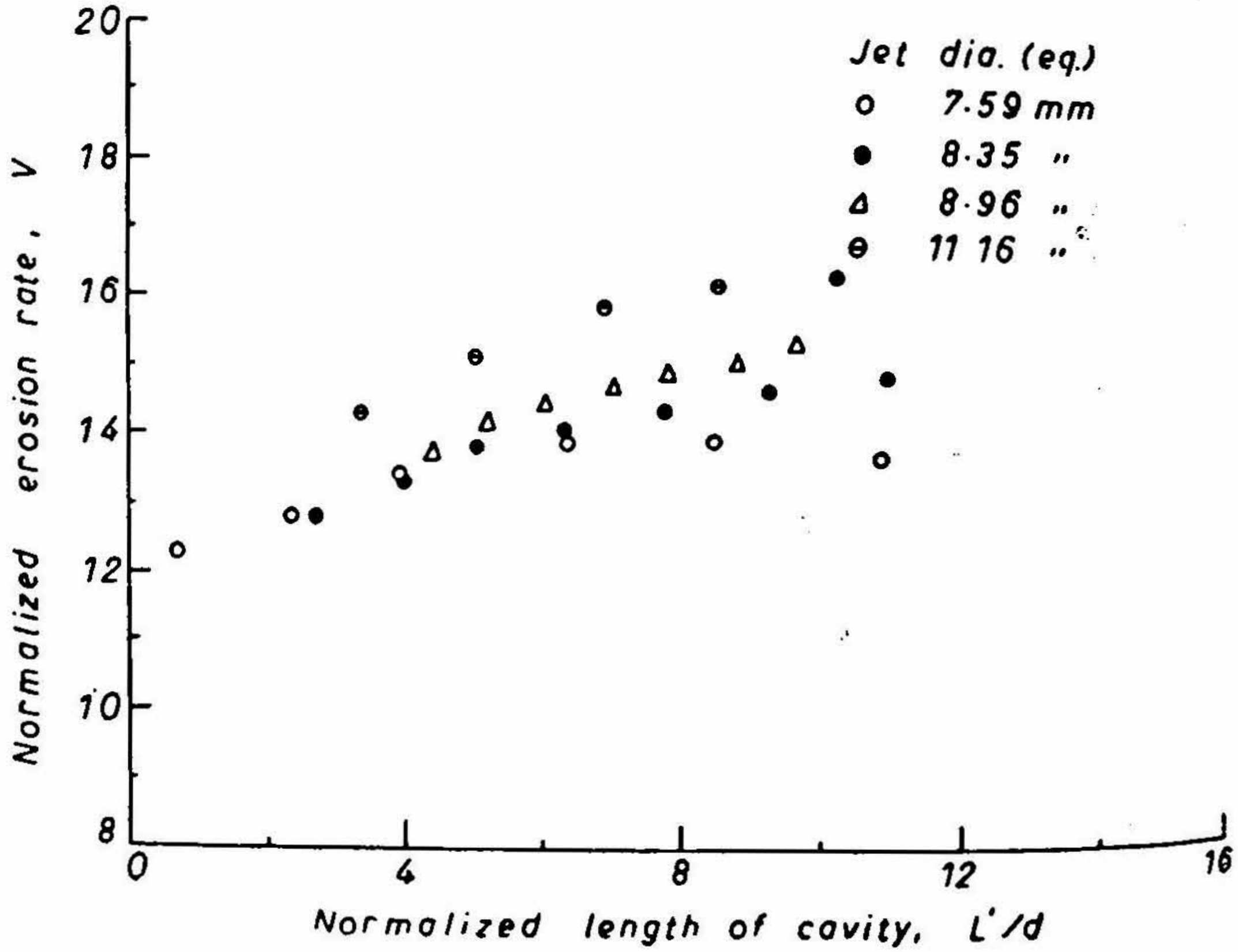

FIG. 21. Variation of normalized erosion rate with length of cavity.

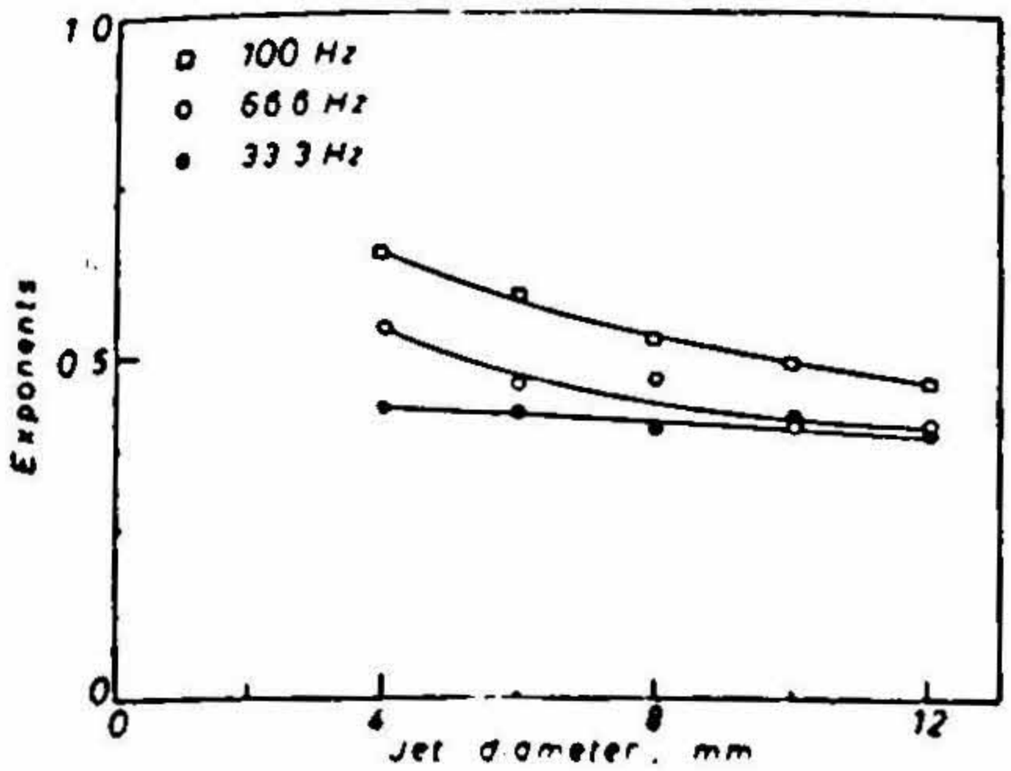

FIG. 22 (*a*). Effect of velocity on erosion data.

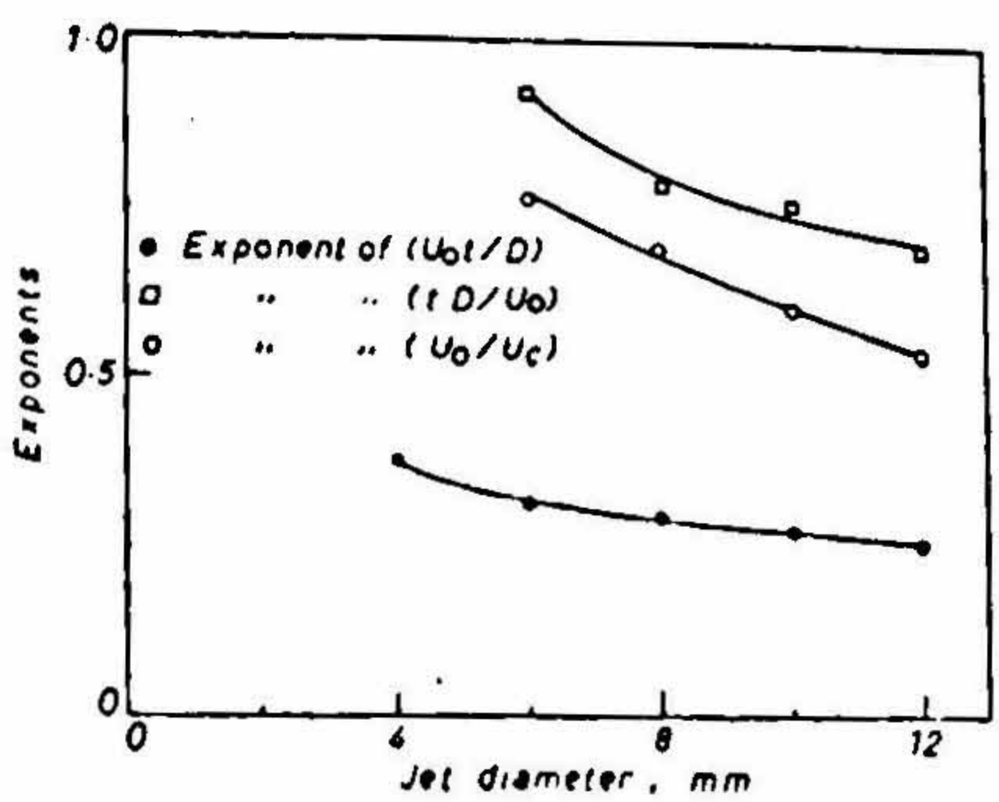

FIG. 22 (*b*). Effect of time frequency and velocity on erosion.

5. Conclusions

(*a*) A detailed dimensional analysis of the several parameters governing liquid impingement erosion resulted in the following relationship :

$$\epsilon = \epsilon\left[\frac{V_t}{\pi/4\, t\, U_0 D^2}, \frac{A_0}{D^2}\right] = \phi\left[\frac{L}{D}, \frac{U_0 t}{D}, \frac{D}{d}, \frac{p_1}{\frac{1}{2}\rho_l U_0^2}, \frac{fD}{U_0}, \theta, \frac{\rho_l}{\rho_s}, \frac{U_0}{e_l}, \frac{\rho_l U_0 D}{\mu}, \frac{M_l}{\rho_l U_0^2}, \frac{U_0}{C_l}\right]$$

(*b*) As the stand-off distance between nozzle and the target is increased, the normalized erosion rate increases to a peak and then decreases. For jets with cavitation inducers the peak volume loss rate occurs at a larger distance than with plain jets.

(*c*) In the case of plain jets, with increase in stand-off distance up to $\sqrt{L/D'} = 2{\cdot}5$, the jet size remained constant. After this the increase in jet size due to spreading with increase in stand-off distance could be expressed by the relationship

$$D'/D = K_1\sqrt{L/D'} + C_1$$

where D' is the jet diameter at any section.

(*d*) The variation of volume loss with jet velocity may be expressed as

$$V_l = K_2 U_0^{m_2}$$

Over the range of impingement frequencies studied, the exponent varies from 3 to 8 for plain jets and from 4 to 9 for jets with cavitation inducers. The normalized erosion rate increases with increase in jet velocity and approaches a constant value at higher jet velocities for plain jets. For jets with cavitation inducers with increase in cavitation number the normalized erosion rate first decreases rapidly and then becomes approximately constant.

(*e*) The normalized erosion rate increases with increase in frequency of impingement for both plain and cavitating jets. This relationship may be expressed as

$$V_1 = K_3 (f/I_0)^n$$

where K_3 is a coefficient and n is an exponent. The exponent varies from 0·16 to 1·75 for plain jets and from 1·02 to 1·47 for cavitating jets. The dimensional quantity volume loss varies as the 4th to 9th power of frequency of impingement, with increase in jet diameter.

(*f*) The erosion rate increases mildly with the angle of impingement. The peak erosion rate attains a maximum value around 25 to 40° of impingement angle.

(*g*) The variation of the relative intensity of erosion with normalized test time in the case of cavitating jets agrees with the theoretical trend suggested by Thiruvengadam[8,18]. The exponent a in the distribution function varies logarithmically with jet velocity for a given frequency of impingement and target material.

(*h*) The cavity patterns obtained for jets with cavitation inducers are similar to those reported in cavitation studies. The length and width of cavity increase with decrease in cavitation number. The increase is rapid at small cavitation numbers and mild at large cavitation numbers.

Acknowledgements

The authors acknowledge with thanks the assistance rendered by Sri N. Balasubramanya, Research Scholar, in computations dealing with regression analysis.

References

1. American Society for Testing Materials—Special Technical Publications :
Erosion and cavitation, ASTM STP 307, 1961.
Erosion by cavitation or impingement, ASTM STP 408, 1967.
Characterization and determination of erosion resistance, ASTM STP 474, 1969.
Erosion, wear and interfaces with corrosion, ASTM STP 567, 1973.

American Society of Mechanical Engineers :
Fluid meters—Their theory and applications, ASME, 1959.
Power test code supplement—Instruments and apparatus, Chapter 4, *Flow measurement*, Part 5.
Measurement of quantity of materials, ASME, 1959.

2. BLOWERS, R. W. On the response of an elastic solid to drop impact, *J. Inst. Math. its Applic.*, 1969, 5(2), 167–193.

3. British Hydromechanic Research Association: *Proceedings of International Symposia on Jet Cutting Technology*, BHRA Fluid Engineering:
First Symposium, Coventry, England, 1972.
Second Symposium, Cambridge, England, 1974.
Third Symposium, Chicago, U.S.A., 1976.
Fourth Symposium, Canterbury, England, 1978.

4. GUTH, W. The formation of pressure waves by cavitation, cavitation in hydrodynamics, *Proc. Symp.* held at NPL, Middlesex, Teddington, Sept. 1955.

5. LECHER, W. Cavitation research on water turbines, *Escher Wyss News*, 1960, 33, nl'2/3, 42-48.

6. JANAKIRAM, K. S. *Studies on the characteristics of erosion due to impingement of plain jets and jets with cavitation inducers*, Ph.D. Thesis, Indian Institute of Science, Bangalore, India, 1978.

7. HAMMITT, F. G. *Droplet impact erosion research—Past and Present*, SOGREAH, Report, NT 1666, Grenoble, France, July 1971.

8. THIRUVENGADAM, A. RUDY, S. L. AND GUNASEKARAN, M. Experimental and analytical investigations on liquid impact erosion, characterization and determination of erosion resistance, ASTM STP 474 Am. Soc. Test. Mat., 1970, pp. 249–281.

9. HEYMANN, F. J. Erosion by cavitation, liquid impingement and solid impingement report E-1460, Westinghouse Electric Corporation, Lester, Pennsylvania, March 1968.

10. FYALL, A. A., KING, R. B. AND STRAIN, R. N. C. Rain erosion aspects of aircraft and guided missiles, *J. R. Aeronaut. Soc.*, 1962, 66, 447–453.

11. JANAKIRAM, K. S. AND SYAMALA RAO, B. C. Studies on the characteristics of erosion with plain jets and jet. with cavitation inducers, *J. Testing Evaluation*, JTEVA, 1978, 6(6), 332–340.

12. FUNDEN WANG, ROBBINS, R. AND OLSEN, J. Water jet assisted tunnel boring, *Proc. Third Int. Symp. on Jet Cutting Technology*, BHRA Fluid Engineering, May 1976, pp. X63–X71.

13. COOLEY, W. C. Survey of water jet coal mining technology, *Proc. Third Int. Symp. on Jet Cutting Technology*, BHRA Fluid Engineering, May 1976, pp. D1–D12.

14. BEUTIN, E. F. *et al.* A new technique in the application of high speed water jet, *Proc. Third Int. Symp. on Jet Cutting Technology*, BHRA Fluid Engineering, May 1976, pp. F2-15 to F2-22.

15. LICHTAROWICZ, A. Experiments with cavitating jets, *Proc. Second Int. Symp. on Jet Cutting Technology*, BHRA Fluid Engineering, Cranfield, April 1974, Paper D1, pp. 1–6.

16. BUSCH, H. *et al.* Rain erosion properties of materials, *Phil. Trans. R. Soc.*, Ser. A, 1966, 260(1110), 168–178.

17. FYALL, A. A., KING, R. B. AND STRAIN, R. N. C. Rain erosion aspects of aircraft ard guided missiles, *J. R. Aeronaut. Soc.*, 1962, 66, 447–453.

18. THIRUVENGADAM, A. *Hand-book of cavitation damage*, Hydronautics, Inc., Tech. Report 233-8, Laurel, Md., March 1965.